# Thermodynamics and fluctuations in finite-time quantum heat engines under reservoir squeezing

Yang Xiao,[1] Dehua Liu,[1] Jizhou He,[1] Lin Zhuang,[2,*] Wu-Ming Liu,[3] L.-L Yan,[4] and Jianhui Wang[1,5,†]

[1]*Department of Physics, Nanchang University, Nanchang 330031, China*

[2]*State Key Laboratory of Optoelectronic Materials and Technologies, School of Physics, Sun Yat-Sen University, Guangzhou 510275, China*

[3]*Beijing National Laboratory for Condensed Matter Physics, Institute of Physics, Chinese Academy of Sciences, Beijing 100190, China*

[4]*School of Physics, Zhengzhou University, Zhengzhou 450001, China*

[5]*State Key Laboratory of Surface Physics and Department of Physics, Fudan University, Shanghai 200433, China*

(Received 1 September 2022; revised 24 February 2023; accepted 23 October 2023; published 27 November 2023)

We investigate the thermodynamics and fluctuations of a finite-time quantum Otto engine alter- natively driven by a hot-squeezed and a cold thermal reservoir. We show that reservoir squeezing significantly enhances the performance by increasing the thermodynamic efficiency and the power and enables higher stability by decreasing the relative power fluctuations and speeding up the convergence of quantum efficiency to its most probable value. We also demonstrate the counterintuitive result that the efficiency can be larger than the Otto limit in the finite-time operation. Experimental demonstration of this quantum heat engine can be available, based on a single-electron spin pertaining to a trapped $^{40}Ca^{+}$ ion [D. von Lindenfels *et al.*, Phys. Rev. Lett. **123**, 080602 (2019)]. We provide a general framework for reliably studying the finite-time nanoengine in finite-time operation which accounts for quantum friction and coherence, deriving important insights into the thermodynamic behaviors beyond the classical thermal machines.

DOI: 10.1103/PhysRevResearch.5.043185

## I. INTRODUCTION

Quantum heat engines have become a laboratory reality, notably the recent experiments realizing quantum Otto heat engines on nuclear magnetic resonance [1,2] and nitrogen-vacancy centers in diamond [3]. These thermal machines wherein, apart from the working substance, the reservoirs may be finite-dimensional and thus nonthermal [4,5], have access to nanoscale open systems in which quantum effects manifest themselves, such as coherence [6–18], entanglement [19–23], correlations [24–27], quantum measurements [28–32], and squeezing [33–39]. The quantum engines in the presence of these additional freedoms may outperform their classical counterparts [10,40–50]. This constitutes one of the central issues in quantum thermodynamics.

For microscopic systems, heat and work are no longer deterministic [51–61], as is the case for macroscopic systems. As a result, the efficiency and power for quantum heat engines are stochastic, and both are fluctuating. The power fluctuations, together with the efficiency fluctuations [62,63], as a limiting factor for the practical usefulness in heat engines, measure the machine stability [53]. Ideally, the quantum heat engine should have high efficiency (small entropy production), large power, and small fluctuations for these thermodynamic variables measuring performance. Strong emphasis has been put on the finite-time thermodynamics of the quantum heat engines and particularly on fluctuations of power and efficiency [63–70].

Unlike the previous studies considering nanoengines [1,2,33,34,48,49,71], where quasistatic and local-equilibrium approximations were required, and thus, some quantum effects were tied to ignoring, we develop a formalism for analyzing the performance and stability for quantum heat engines by overcoming these limitations. We show that both efficiency and power are enhanced by reservoir squeezing with the advantage of decreasing fluctuations of efficiency and power, which is the generic case for finite-time cyclic heat engines driven by nonthermal reservoirs. The result that the efficiency can be enhanced by speeding up the machine even in the absence of squeezing is in stark contrast to previous reports [17,72–74]. We find the counterintuitive result that the efficiency can beat the Otto limit when and only when the unitary driving proceeds in finite time. The result relies only on purely quantum origin, and it would not hold when either unitary driven stroke or thermal-contact process satisfies the quasistatic limit.

## II. FINITE-TIME QUANTUM OTTO ENGINE MODEL

Consider a quantum Otto engine cycle working between a hot-squeezed and a cold thermal bath [see Fig. 1(a)]. This engine cycle consists of two unitary and two isochoric strokes. Firstly, unitary compression from state $\rho_{t_0}$ to $\rho_{t_1}$ with $t_0 = 0$: The energy gap is enlarged by a spin-$\frac{1}{2}$ system with

*stzhl@mail.sysu.edu.cn

†wangjianhui@ncu.edu.cn

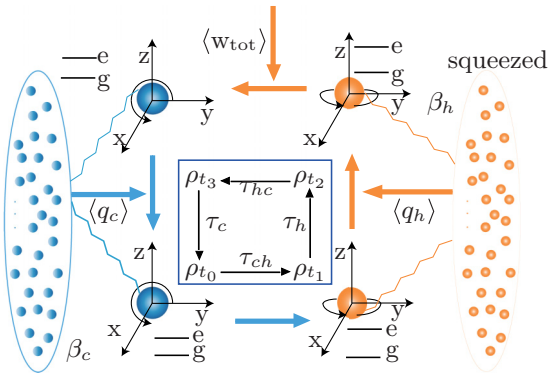


FIG. 1. Illustration of a spin-$\frac{1}{2}$ system operating with a quantum Otto cycle alternatively driven by a hot-squeezed and a cold thermal bath. The system states at times $t = t_i$ with $i = 0, 1, 2,$ and 3 are denoted by $\rho_{t_i}$, where $\rho_{t_i}$ are the initial states of the four strokes in a cycle, respectively. In each cycle, the machine produces the total work $-\langle \mathrm{w_{tot}} \rangle$ by absorbing average heats from the hot and cold baths, $\langle q_h \rangle$ and $\langle q_c \rangle$, where $\langle q_h \rangle = -\langle \mathrm{w_{tot}} \rangle - \langle q_c \rangle$ due to the energy conservation

Hamiltonian $H_{ch}(t) = \frac{\hbar\omega(t)}{2}\{\cos[\pi t/(2\tau_{ch})]\sigma_x + \sin[\pi t/(2\tau_{ch})]\sigma_z\}$, where $\omega(t) = \omega_c(1 - t/\tau_{ch}) + \omega_h(t/\tau_{ch})$, with $\tau_{ch} = t_1$ and $0 \leqslant t \leqslant \tau_{ch}$, and $\sigma_{x,y,z}$ are the Pauli matrices. The driven Hamiltonian does not commute at different times, generating quantum coherence in the energy basis of the system. Secondly, isochoric heating from state $\rho_{t_1}$ to $\rho_{t_2}$: The system is weakly coupled to a hot-squeezed reservoir at inverse temperature $\beta_h$ during time duration $\tau_h$, with $\tau_h = t_2 - t_1$, while its Hamiltonian keeps a constant as $H_h(t) = H_{ch}(t_1) = \hbar\omega_h\sigma_z/2$. Thirdly, unitary expansion from state $\rho_{t_2}$ to $\rho_{t_3}$: The driven Hamiltonian $H_{hc}(t_3 - t) = H_{ch}(t)$ is realized by reversing the protocol used in the unitary compression, such that the expansion Hamiltonian takes the same time as the compression Hamiltonian, namely, $\tau_{\mathrm{dri}} = \tau_{hc} = \tau_{ch}$. Lastly, isochoric cooling from state $\rho_{t_3}$ to $\rho_{t_3+\tau_c}$: The system is weakly coupled with a cold thermal reservoir at inverse temperature $\beta_c$ in time period $\tau_c$, and its Hamiltonian is kept constant at $H_c(t) = H_{ch}(0) = \hbar\omega_c\sigma_x/2$. These times $\tau_h, \tau_c$, and $\tau_{\mathrm{dri}}$ set the total cycle period $\tau_{\mathrm{cyc}}$, namely, $\tau_{\mathrm{cyc}} = \tau_h + \tau_c + 2\tau_{\mathrm{dri}}$. We consider the machine working in the limit cycle [75] where a periodic steady state is achieved with all the periodic variables.

The dynamics of a quantum system weakly coupled to a heat reservoir of inverse temperature $\beta$ can be described by quantum master equation in Lindblad form [76,77]:

$$\frac{d\rho}{dt} = -\frac{i}{\hbar}[H, \rho_t] + \mathcal{L}_D(\rho_t), \tag{1}$$

where $\mathcal{L}_D$ is the Lindblad superoperator describing heat dissipation responsible for driving the system to the thermal equilibrium state, where $\rho_t = \rho_t^{\mathrm{eq}} = e^{-\beta H}/\mathrm{Tr}(e^{-\beta H})$. It is noted that, in the hot isochoric stroke, where the reservoir is squeezed with squeezing parameter $r$, the dynamics in Eq. (1) still holds by setting $\rho_t = \hat{\mathcal{S}}(r)\rho_t\hat{\mathcal{S}}^\dagger(r)$, with $\hat{\mathcal{S}}(r) = \exp(r^*\sigma_- - r\sigma_+)$ being dependent on both $r$ and $\sigma_\pm = (\sigma_x \pm i\sigma_y)/2$. Specifically, in the isochoric stroke where the Hamiltonian is static, the master Eq. (1) turns out to be [77,78]

$$\begin{aligned}\frac{d}{dt}\rho_t &\equiv \mathcal{L}_D^{\mathrm{sq}}(\rho_t)\\ &= \gamma_h(N_h^{\mathrm{ss}} + 1)\left(\sigma_-\rho_t\sigma_+ - \frac{1}{2}\sigma_+\sigma_-\rho_t - \frac{1}{2}\rho_t\sigma_+\sigma_-\right)\\ &\quad + \gamma_h N_h^{\mathrm{ss}}\left(\sigma_+\rho_t\sigma_- - \frac{1}{2}\sigma_-\sigma_+\rho_t - \frac{1}{2}\rho_t\sigma_-\sigma_+\right)\\ &\quad - \gamma_h M\sigma_+\rho_t\sigma_+ - \gamma_h M^*\sigma_-\rho_t\sigma_-,\end{aligned} \tag{2}$$

where we have used

$$N_h^{\mathrm{ss}} = N_h^{\mathrm{th}}[\cosh^2(r) + \sinh^2(r)] + \sinh^2(r) \tag{3}$$

to denote the excitation number of the system, which reaches the steady state with the squeezed bath [77]. Here, $N_h^{\mathrm{th}} = [\exp(\beta_h\hbar\omega_h) - 1]^{-1}$, and $M = -\frac{1}{2}\sinh(2r)e^{i\theta}(2N_h^{\mathrm{th}} + 1)$, with the phase factor $\theta$, and with the vacuum decay rate $\gamma_h$, which indicates the system-bath interaction strength.

From Eq. (2), one can find [78] that the time-dependent state $\rho(t)$ along the hot isochore can be determined according to

$$\rho_t = \begin{pmatrix} \frac{1+\langle\sigma_z(t)\rangle}{2} & \mathcal{X} \\ \mathcal{X}^* & \frac{1-\langle\sigma_z(t)\rangle}{2} \end{pmatrix}, \tag{4}$$

where $\mathcal{X} = \exp(-i\omega_h t)[\exp(\gamma_h a t) + 1]\exp[-\gamma_h(2N_h^{\mathrm{ss}} + 1 + a)t/2]\langle\sigma_-(t_1)\rangle/2 + \sinh(\gamma_h a t/2)\exp[i\theta - \gamma_h(2N_h^{\mathrm{ss}} + 1)t/2]\langle\sigma_+(t_1)\rangle$, with $a = \sinh(2r)(1 + 2N_h^{\mathrm{th}})$, and $\langle\sigma_z(t)\rangle = \exp[-\gamma_h(2N_h^{\mathrm{ss}} + 1)t]\langle\sigma_z(t_1)\rangle - \{1 - \exp[-\gamma_h(2N_h^{\mathrm{ss}} + 1)t]\}/(2N_h^{\mathrm{ss}} + 1)$. The density matrix at the end of hot isochore $\rho_{t_2}$ can be determined by Eq. (4) if we set $t = t_2$.

If the hot isochore is slow enough such that $\tau_h \gg \tau_{h,\mathrm{relax}}$, where $\tau_{h,\mathrm{relax}}$ is the relaxation time of the system with the hot bath, the steady state $\rho_t^{\mathrm{ss}}$ of the system can be reached at the end of this stroke, and it can obtained by setting $d\rho_t^{\mathrm{ss}}/dt = 0$. In such a case, the density matrix Eq. (4) reduces to

$$\rho_h^{\mathrm{ss}} \equiv \rho_{t_2}^{\mathrm{ss}}\Big|_{\tau_h \gg \tau_{h,\mathrm{relax}}} = \begin{pmatrix} p_{t_2}^{e,\mathrm{ss}} & 0 \\ 0 & p_{t_2}^{g,\mathrm{ss}} \end{pmatrix}, \tag{5}$$

where $p_{t_2}^{e,\mathrm{ss}} = N_h^{\mathrm{ss}}/(2N_h^{\mathrm{ss}} + 1)$ and $p_{t_2}^{g,\mathrm{ss}} = 1 - p_{t_2}^{e,\mathrm{ss}}$. If we introduce the effective inverse temperature:

$$\beta_h^{\mathrm{eff}} = \frac{1}{\hbar\omega_h}\ln\frac{N_h^{\mathrm{ss}} + 1}{N_h^{\mathrm{ss}}}, \tag{6}$$

to rewrite the excitation number as $N_h^{\mathrm{ss}} = 1/[\exp(\beta_h^{\mathrm{eff}}\hbar\omega_h) - 1]$, the detailed balance is restored in the squeezing case owing to the relation $\langle e(t_2)|\rho_{t_2}|e(t_2)\rangle/\langle g(t_2)|\rho_{t_2}|g(t_2)\rangle = \exp(-\beta_h^{\mathrm{eff}}\hbar\omega_h)$, with $\tau_h \gg \tau_{h,\mathrm{relax}}$. When $\tau_h \gg \tau_{h,\mathrm{relax}}$, the system could be fully thermalized along the hot isochore, and all the coherence produced in the compression would be erased [see Eq. (5)]. However, for incomplete thermalization with $\tau_h \leqslant \tau_{h,\mathrm{relax}}$, a residual amount of the coherence is retained, and thus, the parameter $\mathcal{X}$ in Eq. (4) is nonzero. Such coherence that endures in this finite-time isochoric process will be present in the next driven stroke.

Along the isochoric cooling stroke, where no squeezing is present and $r = 0$, the dynamics of the state $\rho_t$ is given

by [77]

$$\frac{d}{dt}\rho_t = \gamma_c\left(N_c^{\rm th}+1\right)\left(\sigma_-\rho_t\sigma_+ - \frac{1}{2}\sigma_+\sigma_-\rho_t - \frac{1}{2}\rho_t\sigma_+\sigma_-\right) + \gamma_c N_c^{\rm th}\left(\sigma_+\rho_t\sigma_- - \frac{1}{2}\sigma_-\sigma_+\rho_t - \frac{1}{2}\rho_t\sigma_-\sigma_+\right), \quad (7)$$

where $N_c^{\rm th} = [\exp(\beta_c\hbar\omega_c)-1]^{-1}$ is the excitation number of the system at thermal equilibrium with the cold bath, and $\gamma_c$ is the interaction strength between the system and the cold thermal bath. Using Eq. (7), we can obtain the density operator $\rho_t$ of the system along the cold isochore and then make a unitary transformation of the density matrix from the $\sigma_z$ basis to the $\sigma_x$ basis to arrive at

$$\rho_t = \mathcal{R}\begin{pmatrix} \frac{1+\langle\sigma_z(t)\rangle}{2} & \mathcal{Y}e^{-i\omega_c t} \\ \mathcal{Y}^* e^{i\omega_c t} & \frac{1-\langle\sigma_z(t)\rangle}{2}\end{pmatrix}\mathcal{R}^\dagger, \quad (8)$$

where the transformation matrix $\mathcal{R} = \begin{bmatrix}\langle e(t_1)|e(t_0)\rangle & \langle g(t_1)|e(t_0)\rangle \\ \langle e(t_1)|g(t_0)\rangle & \langle g(t_1)|g(t_0)\rangle\end{bmatrix}$, $\mathcal{Y} = \exp[-\gamma_c(2N_c^{\rm th}+1)t/2]\langle\sigma_-(t_3)\rangle$, and $\langle\sigma_z(t)\rangle = \exp[-\gamma_c(2N_c^{\rm eq}+1)t]\langle\sigma_z(t_3)\rangle - \{1-\exp[-\gamma_c(2N_c^{\rm eq}+1)t]\}/(2N_c^{\rm eq}+1)$. Setting $t=t_0$, the density matrix at the end of cold isochore $\rho_{t_0}$ can be determined by Eq. (8).

When the time duration $\tau_c$ is much larger than the relaxation time $\tau_{c,\rm relax}$, $\mathcal{Y}$ becomes vanishing, and the system reaches thermal equilibrium at the end of the cooling stroke, and then the state of the system takes the form (in the $\sigma_x$ basis):

$$\rho_c^{\rm eq} \equiv \rho_{t_0}\Big|_{\tau_c\gg\tau_{c,\rm relax}} = \begin{pmatrix} \frac{1}{2} & \frac{p_{t_0}^{e,\rm eq}-p_{t_0}^{g,\rm eq}}{2} \\ \frac{p_{t_0}^{e,\rm eq}-p_{t_0}^{g,\rm eq}}{2} & \frac{1}{2}\end{pmatrix}, \quad (9)$$

where $p_{t_0}^{e,\rm eq} = N_c^{\rm eq}/(2N_c^{\rm eq}+1)$ and $p_{t_0}^{g,\rm eq} = 1-p_{t_0}^{e,\rm eq}$.

For a unitary driven stroke where the system is isolated from the heat reservoir, Eq. (1) describing the system dynamics turns out to be $d\rho_t/dt = -\frac{i}{\hbar}[H,\rho_t]$. After obtaining density matrices of the system at the respective ends of the two isohcoric strokes $\rho_{t_2}$ and $\rho_{t_0}$, the system states at the respective ends of the two unitary driven strokes $\rho_{t_1}$ and $\rho_{t_3}$ can be derived by using $\rho_{t_1} = U_{ch}\rho_{t_0}U_{ch}^\dagger$, $\rho_{t_3} = U_{hc}\rho_{t_2}U_{hc}^\dagger$, where $U_{ch} = \mathcal{T}_>\exp\{-\frac{i}{\hbar}\int_{t_0}^{t_1}dtH_{ch}(t)\}$ and $U_{hc} = \mathcal{T}_>\exp\{-\frac{i}{\hbar}\int_{t_2}^{t_3}dtH_{hc}(t)\}$, with the time-ordering operator $\mathcal{T}_>$.

## III. STATISTICS OF HEAT AND WORK

In a realistic scenario, we consider that the interaction between the system and the external field is weak, and the change of internal energy is equal to the work extracted from the system. We then use a full counting statistics method [79,80] to obtain the work distribution along the driving compression as

$$p(\mathrm{w}_{ch}) = \sum_{n,n',m} U_{ch}^{mn}\langle n(t_0)|\rho_{t_0}|n'(t_0)\rangle U_{ch}^{n'm\dagger} \times\delta\left[\mathrm{w}_{ch} - \left(\varepsilon_m^h - \frac{\varepsilon_n^c+\varepsilon_{n'}^c}{2}\right)\right], \quad (10)$$

where we have used $H_{ch}(t_0)|n(t_0)\rangle = \varepsilon_n^c|n(t_0)\rangle$, $H_{ch}(t_0)|n'(t_0)\rangle = \varepsilon_{n'}^c|n'(t_0)\rangle$, $H_{ch}(t_1)|m(t_1)\rangle = \varepsilon_m^h|m(t_1)\rangle$, $U_{ch}^{mn} = \langle m(t_1)|U_{ch}|n(t_0)\rangle$, and $U_{ch}^{n'm\dagger} = \langle n'(t_0)|U_{ch}^\dagger|m(t_1)\rangle$. Here, the term $|\langle n(t_0)|U_{ch}|m(t_1)\rangle|^2$ denotes the transition probability between the system eigenstates $|n(t_0)\rangle$ and $|m(t_1)\rangle$, and $\langle n(t_0)|\rho_{t_0}|n(t_0)\rangle$ is the probability of the system being in state $|n(t_0)\rangle$. For the two-level system under consideration, we use $|g\rangle$ and $|e\rangle$ $(n,m=g,e)$ to denote the ground and excited eigenstates, respectively. When the driven stroke is quantum adiabatic, transition between any two eigenstates will not happen, and therefore, $|\langle n(t_0)|U_{ch}|m(t_1)\rangle|^2 = \delta_{nm}$. However, along the finite-time driven stroke, the inner friction causes the transitions among the instantaneous energy eigenstates, resulting in the irreversible work.

As no work is produced along the hot isochoric process, the stochastic heat injection is equivalent to the increase of the system eigenenergy. The transition probability from eigenstate $k$ to $l$ along the hot isochore $|\langle k(t_1)|U_h(t)|l(t_2)\rangle|^2$, with the time evolution operator $U_h(t)$, can be obtained by using $\rho_t = U_h|k(t_1)\rangle\langle k(t_1)|U_h^\dagger$ to arrive at $|\langle k(t_1)|U_h(t)|l(t_2)\rangle|^2 = \langle l|\rho_t|l\rangle$. Using $H_h(t)|l(t_2)\rangle = \varepsilon_l^h|l(t_2)\rangle$ and $H_h(t)|k(t_1)\rangle = \varepsilon_k^h|k(t_1)\rangle$, it follows that the probability distribution for the heat absorbed during this stroke reads

$$p(q_h|\mathrm{w}_{ch}) = \sum_{k,l}\delta\left[q_h - \left(\varepsilon_l^h - \varepsilon_k^h\right)\right]\langle l(t_2)|\rho_{t_2}|l(t_2)\rangle\delta_{km}, \quad (11)$$

where $\langle l(t_2)|\rho_{t_2}|l(t_2)\rangle$ is the probability of finding the system to be in eigenstate $|l(t_2)\rangle$.

Like in the first stroke, the internal friction (due to finite time evolution) will bring coherence and result in the transition between the eigenstates of the Hamiltonian $H_{hc}(t_3)$ and $H_{hc}(t_2)$. The quantum work distribution along the driven stroke can be expressed as

$$p(\mathrm{w}_{hc}|\mathrm{w}_{ch},q_h) = \sum_{i,i',j} U_{hc}^{j,i}\langle i(t_2)|\rho_{t_2}|i'(t_2)\rangle U_{hc}^{i'j\dagger} \times\delta\left[\mathrm{w}_{hc} - \left(\varepsilon_j^c - \frac{\varepsilon_i^h+\varepsilon_{i'}^h}{2}\right)\right]\delta_{i,l}, \quad (12)$$

where we have used $H_{hc}(t_2)|i(t_2)\rangle = \varepsilon_i^h|i(t_2)\rangle$, $H_{hc}(t_2)|i'(t_2)\rangle = \varepsilon_{i'}^h|i'(t_2)\rangle$, $H_{hc}(t_3)|j(t_3)\rangle = \varepsilon_j^c|j(t_3)\rangle$, $U_{hc}^{ji} = \langle j(t_3)|U_{hc}|i(t_2)\rangle$, and $U_{hc}^{i'j} = \langle i'(t_2)|U_{hc}^\dagger|j(t_3)\rangle$. The term $|\langle i(t_2)|U_{hc}|j(t_3)\rangle|^2$ is the transition probability from state $|i(t_2)\rangle$ to $|j(t_3)\rangle$, and $\langle i(t_2)|\rho_{t_2}|i'(t_2)\rangle\delta_{i,i'}$ denotes the probability for finding the system in state $|i\rangle$.

The stochastic work extracted from the system in a single cycle is $-\mathrm{w}_{\rm tot} = -(\mathrm{w}_{ch}+\mathrm{w}_{hc})$, and the stochastic efficiency reads $\eta = -\mathrm{w}_{\rm tot}/q_h$. The joint distribution for the work output $\mathrm{w}_{ch}$, $\mathrm{w}_{hc}$ and heat $q_h$ can be determined according to Eqs. (10), (11), and (12) to arrive at

$$\begin{aligned} p(\mathrm{w}_{ch},q_h,\mathrm{w}_{hc}) &= p(\mathrm{w}_{hc}|\mathrm{w}_{ch},q_h)p(q_h|\mathrm{w}_{ch})p(\mathrm{w}_{ch}) \\ &= \sum_{n,n',m,i,i',j}\delta\left[\mathrm{w}_{ch} - \left(\varepsilon_m^h - \frac{\varepsilon_n^c+\varepsilon_{n'}^c}{2}\right)\right] \\ &\quad\times\delta\left[q_h - \left(\varepsilon_i^h - \varepsilon_m^h\right)\right] \\ &\quad\times\delta\left[\mathrm{w}_{hc} - \left(\varepsilon_j^c - \frac{\varepsilon_i^h+\varepsilon_{i'}^h}{2}\right)\right] \\ &\quad\times U_{ch}^{mn}\langle n(t_0)|\rho_{t_0}|n'(t_0)\rangle U_{ch}^{n'm\dagger} \\ &\quad\times U_{hc}^{ji}\langle i(t_2)|\rho_{t_2}|i'(t_2)\rangle U_{hc}^{i'j\dagger}. \end{aligned} \quad (13)$$

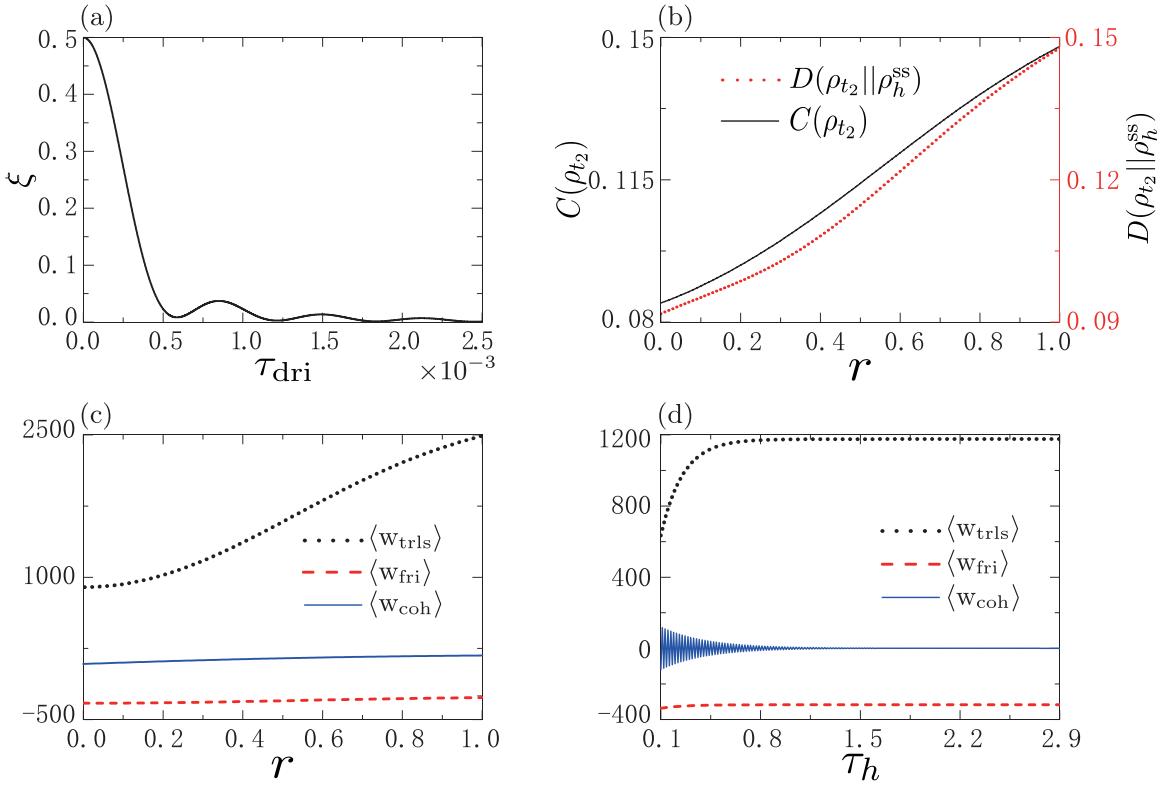


FIG. 2. (a) Transition probability as a function of driving time $\tau_{\rm dri}$. (b) Coherence and Kullback-Leibler divergence at $t = t_2$, with $\tau_h = 0.2$ and $\tau_{\rm dri} = 5 \times 10^{-4}$. (c) Transitionless work, frictional work, and coherent work as a function of squeezing parameter $r$ with $\tau_h = 0.2$, $\tau_{\rm dri} = 5 \times 10^{-4}$; (d) Transitionless work, frictional work, and coherent work as a function of thermal-contact time with $\tau_{\rm dri} = 5 \times 10^{-4}$, $r = 0$. The parameters are $\hbar = 1$, $\omega_c/2\pi = 1000$, $\omega_h/2\pi = 2250$, $\beta_c = 2/(\hbar\omega_c)$, $\beta_h = 1/(\hbar\omega_h)$, $\tau_c = 3$, and $\gamma_c = \gamma_h = 3$.

This sets the joint distribution of the total work $\mathrm{w}_{\rm tot}$ for a cycle with quantum heat injection $q_h$:

$$p(q_h, \mathrm{w}_{\rm tot}) = \int d\mathrm{w}_{ch} d\mathrm{w}_{hc} \delta[\mathrm{w}_{\rm tot} - (\mathrm{w}_{ch} + \mathrm{w}_{hc})] \times p(\mathrm{w}_{ch}, q_h, \mathrm{w}_{hc}). \tag{14}$$

Based on Eq. (14), we find that the average work $\langle \mathrm{w}_{\rm tot}\rangle$, average injection $\langle q_h\rangle$, and work fluctuations $\delta \mathrm{w}_{\rm tot}^2 = \langle \mathrm{w}_{\rm tot}^2\rangle - \langle \mathrm{w}_{\rm tot}\rangle^2$ are given by

$$\begin{aligned} -\langle \mathrm{w}_{\rm tot}\rangle &= \hbar(\omega_h - \omega_c)(\langle n_{t_2}\rangle - \langle n_{t_0}\rangle) \\ &\quad + 2\hbar\xi(\omega_c\langle n_{t_2}\rangle + \omega_h\langle n_{t_0}\rangle) \\ &\quad - 2\hbar\omega_h\zeta_{ch} - 2\hbar\omega_c\zeta_{hc}, \end{aligned} \tag{15}$$

$$\langle q_h\rangle = \hbar\omega_h[\langle n_{t_2}\rangle + \langle n_{t_0}\rangle(2\xi - 1) - 2\zeta_{ch}], \tag{16}$$

$$\begin{aligned} \delta \mathrm{w}_{\rm tot}^2 &= \hbar^2\omega_h^2\{\tfrac{1}{2} - \langle n_{t_2}\rangle^2 - [\langle n_{t_0}\rangle(1-2\xi) + 2\zeta_{ch}]^2\} \\ &\quad + \hbar^2\omega_c^2\{\tfrac{1}{2} - \langle n_{t_0}\rangle^2 - [\langle n_{t_2}\rangle(1-2\xi) + 2\zeta_{hc}]^2\} \\ &\quad + \hbar^2\omega_c\omega_h\{2\langle n_{t_0}\rangle[\langle n_{t_0}\rangle(1-2\xi) + 2\zeta_{ch}] \\ &\quad + 2\langle n_{t_2}\rangle[\langle n_{t_2}\rangle(1-2\xi) + 2\zeta_{hc}] + 2\xi - 1\}, \end{aligned} \tag{17}$$

where we have used $\langle n_{t_i}\rangle := \mathrm{Tr}(\rho_{t_i} H)/(\hbar\omega_i)$, with $\omega_h = \omega_2$ and $\omega_c = \omega_0$, to denote the average populations at times $t = t_i$. Here, $\zeta_{ch} := -\mathrm{Re}[U_{ch}^{gg}\rho_{t_0}^{mn}U_{ch}^{eg\dagger}]$, $\zeta_{hc} := -\mathrm{Re}[U_{hc}^{gg}\rho_{t_2}^{ij}U_{hc}^{eg\dagger}]$, and $\xi \equiv |\langle n(t_0)|U_{ch}|m(t_1)\rangle|^2 = |\langle i(t_2)|U_{hc}|j(t_3)\rangle|^2$, with $U_{ch,hc}^{mn} = \langle m(t_{1,3})|U_{ch,hc}|n(t_{0,2})\rangle (m, n, i, j = e, g)$. The detailed derivation of Eqs. (15), (16), and (17) is presented in Appendix A. The Hamiltonian-dependent parameter $\xi$ that denotes the level transition probability [1] during expansion or compression for the spin system decreases with increasing driving time $\tau_{\rm dri}$, though not monotonically, and it tends to be zero when the time is long enough to satisfy quantum adiabatic condition, as shown in Fig. 2(a).

The parameters $\zeta_{hc}$ and $\zeta_{ch}$ in Eq. (15) are associated with the quantum coherence, of which the amount is quantified by the relative entropy of coherence [81]: $C(\rho) = S[\mathcal{E}(\rho)] - S(\rho)$(with $S(\rho) = -\mathrm{Tr}[\rho\ln\rho]$). Here, $\mathcal{E}(\cdot) = \sum_n \Pi_n(\cdot)\Pi_n$ is the dephasing map by removing all coherence in the energy basis, with $\Pi_n := |n\rangle\langle n|$ being the projection operator of $\rho$. The residual coherence at the end of the hot isochore $C(\rho_{t_2})$ increases as $r$ increases, as shown in Fig. 2(b), where the relative entropy $D(\rho_{t_2}||\rho_h^{\rm ss}) = \mathrm{Tr}[\rho_{t_2}(\ln\rho_{t_2} - \ln\rho_h^{\rm ss})]$, with $\rho_h^{\rm ss} = \rho_{t_2}^{\rm ss}$, increases with increasing $r$, as it should. Quantum coherence generated during in the unitary expansion (compression) interferes with residual coherence after the finite-time hot (cold) isochore. To reveal the effect of such a dynamical interference on the thermodynamic quantities of the machine, our quantum engine is compared with an alternative cycle, where a full dephasing operation [8] is performed to completely remove all coherence after the hot isochore with any value of thermal-contact time $\tau_h$. In what follows, we use the superscript deph to describe the quantities corresponding to the dephased engine cycle.

The average work $-\langle \mathrm{w}_{\mathrm{tot}}\rangle$ in Eq. (15) can be split up into the two terms: $-\langle \mathrm{w}_{\mathrm{tot}}\rangle = \langle \mathrm{w}_{\mathrm{deph}}\rangle + \langle \mathrm{w}_{\mathrm{coh}}\rangle$, where $\langle \mathrm{w}_{\mathrm{deph}}\rangle = \langle \mathrm{w}_{\mathrm{trls}}\rangle + \langle \mathrm{w}_{\mathrm{fri}}\rangle$, with $\langle \mathrm{w}_{\mathrm{trls}}\rangle =: \hbar(\omega_h - \omega_c)(\langle n_{t_2}\rangle - \langle n_{t_0}\rangle)$ and $\langle \mathrm{w}_{\mathrm{fri}}\rangle =: 2\hbar\xi(\omega_c\langle n_{t_2}\rangle + \omega_h\langle n_{t_0}\rangle)$, is the average work in the dephasing case, and $\langle \mathrm{w}_{\mathrm{coh}}\rangle = -2\hbar\omega_h\zeta_{ch} - 2\hbar\omega_c\zeta_{hc}$ is the average work associated with quantum coherence. Here, $\langle \mathrm{w}_{\mathrm{trls}}\rangle$ indicates the work in the transitionless case, where the transitions in the instantaneous energy eigenstates are removed, and $\langle \mathrm{w}_{\mathrm{fri}}\rangle$ represents the additional work that overcomes the inner friction causing unwanted diabatic transitions in instantaneous energy eigenstates. The squeezing results in an increase in the transitionless work and the coherent work but a decrease in the amount of frictional work which is always negative, as shown in Fig. 2(c). The transitionless work $\langle \mathrm{w}_{\mathrm{trls}}\rangle$ increases with increasing thermal-contact time $\tau_h$ to reach the maximum value at which the system approaches the thermal state, but the effects of $\tau_h$ on both frictional work $\langle \mathrm{w}_{\mathrm{fri}}\rangle$ and coherent work $\langle \mathrm{w}_{\mathrm{coh}}\rangle$ are particularly small, as shown in Fig. 2(d). The coherent work displays the oscillations in quick isochoric stroke since the coherence $C(\rho_{t_2})$, which interferes with the coherence generated during the unitary expansion, is only partially erased.

## IV. EFFICIENCY BOUND AND STATISTICS

When the open quantum system evolves along an isochoric process, the external field is frozen, and the control parameter is fixed, leading to a static system Hamiltonian $H(t) = H$. The irreversibility of this system can be well described by the so-called nonadiabatic entropy production rate:

$$\langle \dot{\Sigma}\rangle = -\frac{d}{dt}D\big(\rho_t\big|\big|\rho_t^{\mathrm{ss}}\big) = \dot{S}_t - \dot{\Psi}_t, \tag{18}$$

where $D(\rho_t||\rho_t^{\mathrm{ss}}) = \mathrm{Tr}[\rho_t(\ln\rho_t - \ln\rho_t^{\mathrm{ss}})]$ is the Kullback-Leibler-Umegaki divergence (also called the relative entropy) [82]. In Eq. (18), $\dot{S}_t$ can be given by $\dot{S}_t = -\mathrm{Tr}(\dot{\rho}_t\ln\rho_t + \dot{\rho}_t) = -\mathrm{Tr}(\dot{\rho}_t\ln\rho_t)$, and it indicates the rate of change of the von Neumann entropy of the system $S_t = -\mathrm{Tr}(\rho_t\ln\rho_t)$. The second contribution $\dot{\Psi}$, called the excess entropy production rate, is determined by [83] $\dot{\Psi} = -\mathrm{Tr}(\dot{\rho}_t\ln\rho_t^{\mathrm{eq}})$, which defines the effective rate of entropy flow into the system from its surroundings. Under squeezing, this excess entropy production rate can be expressed as $\dot{\Psi}^{\mathrm{sq}} = -\mathrm{Tr}(\dot{\rho}_t\ln\rho_t^{\mathrm{ss}})$.

The working substance returns to its initial state after a single cycle, and thus, its entropy change is zero [8], which means $\int_0^{\tau_{\mathrm{cyc}}}\dot{S}(t)dt = 0$, with $\tau_{\mathrm{cyc}} = \tau_h + \tau_c + 2\tau_{\mathrm{dri}}$. We therefore find that, for the cyclic engine, the nonadiabatic entropy $\langle\Sigma\rangle$ is equivalent to the excess entropy, and it is coming exclusively from the two system-bath interaction intervals. As emphasized, the working system in the long time intervals of system-bath interaction should reach the thermal state $\rho_c^{\mathrm{eq}}$ in Eq. (9) in the absence of reservoir squeezing or steady state $\rho_h^{\mathrm{ss}}$ in Eq. (5) in the presence of squeezing. For the engine cycle, the total entropy production turns out to be $\langle\Sigma_{\mathrm{tot}}\rangle = \int_0^{\tau_{\mathrm{cyc}}}\langle\dot{\Sigma}\rangle dt = -\int_{t_1}^{t_2}\dot{\Psi}^{\mathrm{sq}}dt - \int_{t_3}^{\tau_{\mathrm{cyc}}}\dot{\Psi}dt$.

Hence, the irreversible production $\langle\Sigma_{\mathrm{tot}}\rangle$ of the cycle can be calculated as $\langle\Sigma_{\mathrm{tot}}\rangle = [\mathrm{Tr}(\rho_{t_2}\ln\rho_h^{\mathrm{ss}}) - \mathrm{Tr}(\rho_{t_1}\ln\rho_h^{\mathrm{ss}})] + [\mathrm{Tr}(\rho_{t_0}\ln\rho_c^{\mathrm{eq}}) - \mathrm{Tr}(\rho_{t_3}\ln\rho_c^{\mathrm{eq}})]$. It then follows that the total entropy production is given by

$$\begin{aligned}\langle\Sigma_{\mathrm{tot}}\rangle &= -\beta_h^{\mathrm{eff}}[\mathrm{Tr}(\rho_{t_2}H_h) - \mathrm{Tr}(\rho_{t_1}H_h)]\\ &\quad - \beta_c[\mathrm{Tr}(\rho_{t_0}H_c) - \mathrm{Tr}(\rho_{t_3}H_c)]\\ &= -\beta_h^{\mathrm{eff}}\langle q_h\rangle - \beta_c\langle q_c\rangle,\end{aligned} \tag{19}$$

where we have used $\langle q_h\rangle = \mathrm{Tr}(\rho_{t_2}H_h) - \mathrm{Tr}(\rho_{t_1}H_h)$ and $\langle q_c\rangle = \mathrm{Tr}(\rho_{t_0}H_c) - \mathrm{Tr}(\rho_{t_3}H_c)$. By very simple algebra, the total entropy production in Eq. (19) can be rewritten as $\langle\Sigma_{\mathrm{tot}}\rangle = D(\rho_{t_0}||\rho_{t_0}^{\mathrm{eq}}) + D(\rho_{t_2}||\rho_{t_2}^{\mathrm{ss}}) - D(\rho_{t_1}||\rho_{t_1}^{\mathrm{ss}}) - D(\rho_{t_3}||\rho_{t_3}^{\mathrm{eq}}) = D[\mathcal{E}(\rho_{t_0})||\rho_{t_0}^{\mathrm{eq}}] + C(\rho_{t_0}) + D[\mathcal{E}(\rho_{t_2})||\rho_{t_2}^{\mathrm{ss}}] + C(\rho_{t_2}) - D[\mathcal{E}(\rho_{t_1})||\rho_{t_1}^{\mathrm{ss}}] - C(\rho_{t_1}) - D[\mathcal{E}(\rho_{t_3})||\rho_{t_3}^{\mathrm{eq}}] - C(\rho_{t_3})$. Using Eq. (19), we derive the machine efficiency as $\eta_{\mathrm{th}} = 1 + \langle q_c\rangle/\langle q_h\rangle = 1 - (\beta_h^{\mathrm{eff}}\langle q_h\rangle + \langle\Sigma_{\mathrm{tot}}\rangle)/(\beta_c\langle q_h\rangle)$, where $\beta_h^{\mathrm{eff}}$, defined by Eq. (6), is given by $\beta_h^{\mathrm{eff}} = \ln(\{2\cosh 2r + [\exp(\beta_h\hbar\omega_h) - 1](\cosh 2r + 1)\}/\{2\cosh 2r + [\exp(\beta_h\hbar\omega_h) - 1](\cosh 2r - 1)\})/(\hbar\omega_h)$.

Introducing the so-called generalized efficiency $\eta_C^{\mathrm{gen}} = 1 - \beta_h^{\mathrm{eff}}/\beta_c$, we then obtain

$$\eta_{\mathrm{th}} = \eta_C^{\mathrm{gen}} - \frac{\langle\Sigma_{\mathrm{tot}}\rangle}{\beta_c\langle q_h\rangle}, \tag{20}$$

which is bounded by the generalized Carnot efficiency $\eta_C^{\mathrm{gen}} = 1 - \beta_h^{\mathrm{eff}}/\beta_c$ due to positive entropy production $\langle\Sigma_{\mathrm{tot}}\rangle$ and average heat injection $\langle q_h\rangle$, as it should be. In the limit of either high temperature or small squeezing, $\eta_{\mathrm{th}} = \sinh(2r)\eta_C - \Sigma_{\mathrm{tot}}/(\beta_c\langle q_h\rangle)$, where $\eta_C = 1 - \beta_h/\beta_c$, showing that the reservoir squeezing improves the efficiency, but the irreversible entropy production deteriorates the performance. Since the system state may not be thermal even in the quasistatic limit, the efficiency is irrelevant to the Carnot bound, and it is bounded by the generalized Carnot value $\eta_C^{\mathrm{gen}}$ due to positive entropy production $\Sigma_{\mathrm{tot}}$ and average heat injection $\langle q_h\rangle$. While this efficiency in Eq. (20) is irrelevant to the Carnot bound [7], another type of the efficiency, in which excess work and housekeeping heat is introduced to consider the additional energy cost for maintaining reservoir squeezing, is bounded by the Carnot value (see Appendix B for details).

By using Eqs. (15) and (16), we derive the thermodynamic efficiency $\eta_{\mathrm{th}} = -\langle \mathrm{w}_{\mathrm{tot}}\rangle/\langle q_h\rangle$ to obtain

$$\eta_{\mathrm{th}} = \eta_{\mathrm{Otto}} + 2(\omega_c/\langle q_h\rangle)[\xi(\langle n_{t_0}\rangle + \langle n_{t_2}\rangle) - \zeta_{hc} - \zeta_{ch}], \tag{21}$$

where $\eta_{\mathrm{Otto}} = 1 - \omega_c/\omega_h$ is the so-called Otto efficiency. Because the times taken for two isochoric and two unitary strokes are finite, the quantum coherence and inner friction are created, resulting in that the efficiency depends on both these two kinds of quantum effects. Quite interestingly, the efficiency $\eta_{\mathrm{th}}$ for the heat engine may surpass the Otto efficiency $\eta_{\mathrm{Otto}}$ [1], if $\xi(\langle n_{t_0}\rangle + \langle n_{t_2}\rangle) > \zeta_{hc} + \zeta_{ch}$. It is of interest to note the two cases (see Appendix C): (i) While the efficiency is independent of squeezing in the case of large difference between two reservoir temperatures, it is sensitively dependent on the squeezing parameter $r$ in the linear response regime, where the difference between two reservoir temperatures is small; (ii) the efficiency depends on the degree of squeezing in the low-temperature and high-temperature limits.

In contrast to the average work, the average efficiency of the quantum Otto engine may be ill defined due to the possible divergence of the stochastic efficiency [63,64]. Hence, we resort to large deviation theory associated with the exponential

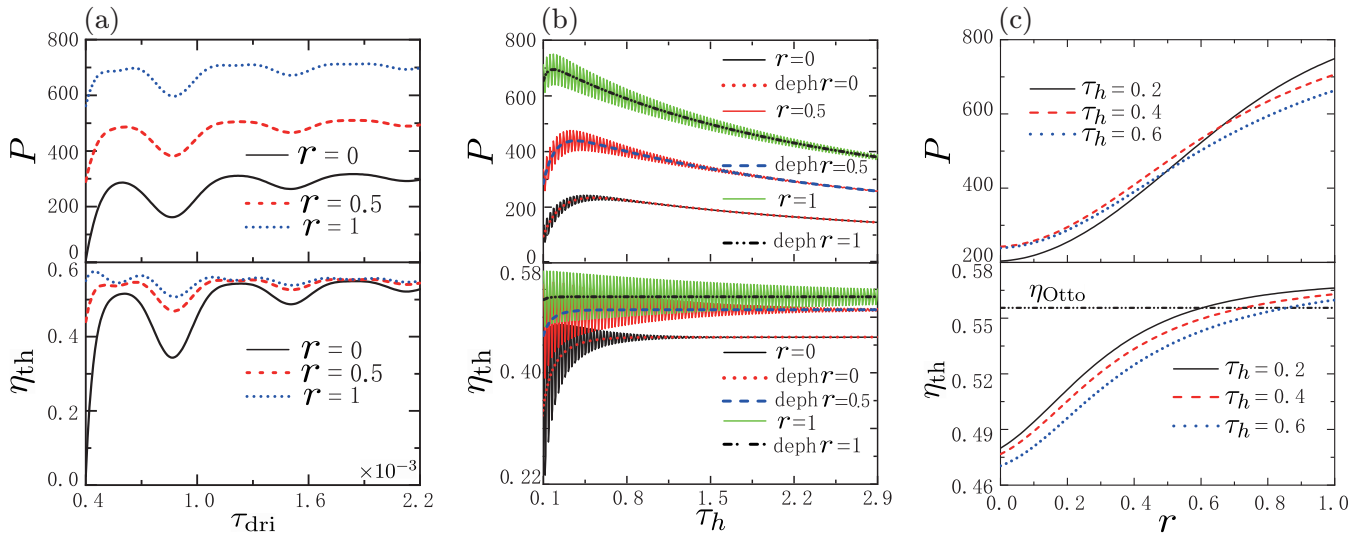


FIG. 3. (a) Power (up) and thermodynamic efficiency (bottom) as a function of driving time with $\tau_h = 0.5$. (b) Power (up) and thermodynamic efficiency (bottom) as a function of thermal-contact time with $\tau_{\rm dri} = 0.0005$. (c) Power (up) and efficiency (bottom) as a function of squeezing parameter with given $\tau_h$ under $\tau_{\rm dri} = 0.0005$. In (b), the dephased engine cycles (labeled deph) are indicated by the red dotted line, blue dashed line, and black dot-dashed line, respectively. The other parameters are same as in Fig. 2.

decay of probabilities of large fluctuations, assuming that the quantum engine proceeds in the long time limit.

We use large deviation theory [59] to analyze the efficiency statistics. We recall that the large deviation functions of the joint distribution $p(q_h, \mathrm{w}_{\rm tot})$ and the efficiency distribution $p_K(\eta)$ for a large number of cycles ($K \gg 1$) are governed by the respective asymptotic forms of $p_K(q_h, \mathrm{w}_{\rm tot}) \asymp \exp[-KI(q_h, \mathrm{w}_{\rm tot})]$, and $p_K(\eta) \asymp e^{-KJ(\eta)}$. The large deviation functions $I(q_h, \mathrm{w}_{\rm tot})$ and $J(\eta)$ describe the exponentially unlikely deviations of $q_h$, $\mathrm{w}_{\rm tot}$, and $\eta$ from their most probable values. The rate function $J(\eta)$ can be obtained from $I(q_h, \mathrm{w}_{\rm tot})$ by the contraction $J(\eta) = \min_{q_h} I(q_h, -\eta q_h)$. When defining $q_h^{(K)} := \sum_{j=1}^{K} q_h^{(j)}/K$, $\mathrm{w}^{(K)} := \sum_{j=1}^{K} \mathrm{w}_{\rm tot}^{(j)}/K$ [60,61], we have $\phi(\varphi_1, \varphi_2) = \lim_{K\to\infty} \frac{1}{K} \ln\langle \exp\{K[\varphi_1 q_h^{(K)} + \varphi_2 \mathrm{w}^{(K)}]\}\rangle = \ln\langle \exp(\varphi_1 q_h + \varphi_2 \mathrm{w}_{\rm tot})\rangle$, where we have used $\langle \exp(\varphi_1 q_h + \varphi_2 \mathrm{w}_{\rm tot})\rangle = \iint dq_h d\mathrm{w}_{\rm tot} \exp(\varphi_1 q_h + \varphi_2 \mathrm{w}_{\rm tot}) p(q_h, \mathrm{w}_{\rm tot})$. Using the Legendre-Fenchel transform, one then obtains the large deviation function of quantum efficiency as

$$J(\eta) = -\min_{\varphi_2} \phi(\varphi_2 \eta, \varphi_2), \tag{22}$$

where $\phi(\varphi_1, \varphi_2) = \ln\langle \exp(\varphi_1 q_h + \varphi_2 \mathrm{w}_{\rm tot})\rangle$.

## V. NUMERICAL RESULTS FOR EFFICIENCY AND POWER

In Fig. 3(a), the power oscillates as a function of the driving time $\tau_{\rm dri}$, and very quick driving speed results in poor power output. In our model, where the driving time $\tau_{\rm dri}$ is much smaller than the thermal-contact time $\tau_h$ ($\tau_c$), and thus, the total cycle period $\tau_{\rm cyc}$ is dominated by $\tau_{h,c}$, the contribution of the driving time to the power mainly comes from quantum inner friction which is responsible for irreversible work. The efficiency increases with increasing driving time, although not monotonically.

We observe from Fig. 3(b) that the power first increases in small $\tau_h$ and then decreases with further increase in $\tau_h$. During the fast hot isochoric stroke, the decoherence of the system is suppressed, yielding the additional, coherent work $\langle \mathrm{w}_{\rm coh}\rangle$ which is responsible for the oscillation. Because the transitionless work $\langle \mathrm{w}_{\rm trls}\rangle$ dominating the total work increases faster than linearly with increasing $\tau_h$, the power increases with increasing $\tau_h$ to a certain maximum value and then decreases gradually. The shapes of the efficiency and power curves are similar, except that $\eta_{\rm th}$ increases with $\tau_h$ to reach its maximum value consistent with $\eta_C^{\rm gen}$. Interestingly, in the large squeezing case, ($r = 1$) leads to large coherence [see Fig. 2(b)] and thus large interference effect, which accounts for large oscillations of the power and efficiency, but these two performance measures become equivalent to their respective dephased counterparts in the long time $\tau_h$, where coherence is full erased, as they should be [see Fig. 2(d)]. By suitably controlling over the driving and thermalization times, the quantum engine may run in a favorable regime where both efficiency and power can be enhanced, as shown in Fig. 3(b).

The coherent work $\langle \mathrm{w}_{\rm coh}\rangle$ in Fig. 2(d) may contribute to the increase of the extracted net work. If the machine parameters are properly adjusted, the faster the unitary and thermal-contact processes are performed, the greater the contribution of the coherence to the total work extracted since coherent work increases with speeding up these processes. The increase of the extracted work with shortening of time may lead to increase power [see Fig. 3(c) (up)] and, surprisingly, causes efficiency to surpass the Otto limit that is reached when coherence is fully erased, or it is not generated along the unitary stroke. Thus, the main message from Fig. 3(c) (bottom), confirms our theoretical prediction in Eq. (21) that quantum coherence, of purely quantum origin, can lead to a marked difference in machine performance.

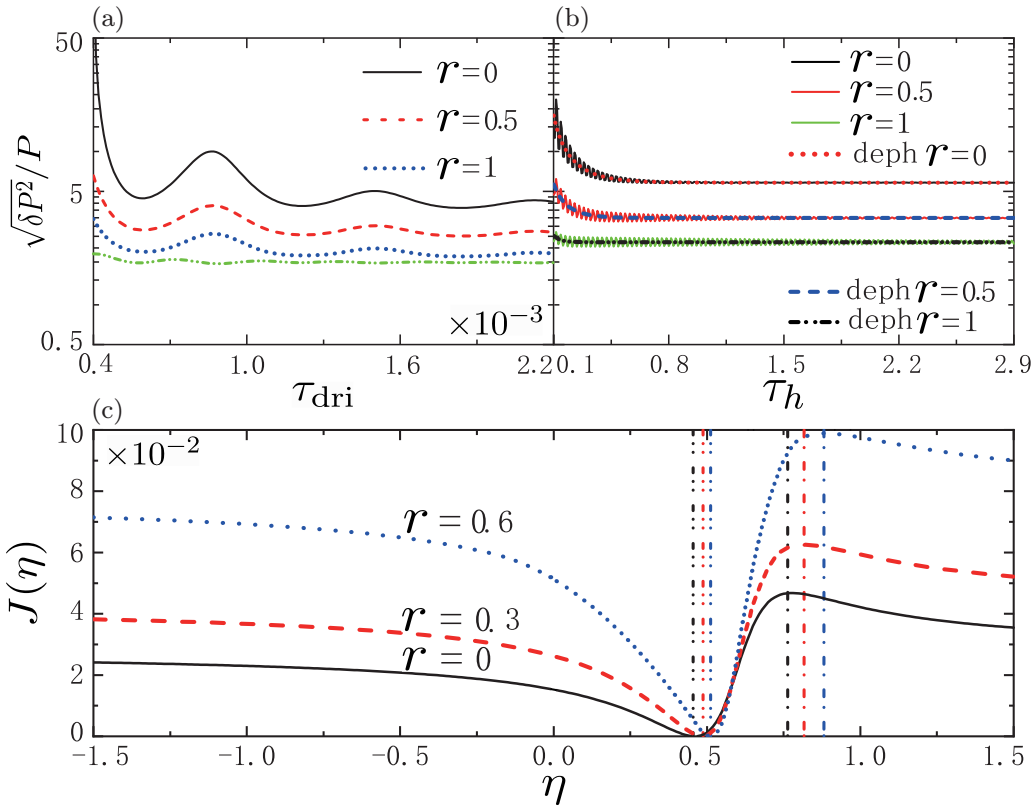


FIG. 4. Root-mean-square relative fluctuation of power $\sqrt{\delta P^2}/P$ as functions of (a) driving time $\tau_{\rm dri}$ and (b) thermalization time $\tau_h$. In (a), the green dash-dotted line indicates the lower bound csch$[f(\langle\Sigma\rangle)]$ (dot-dot-dash line), where $f(\langle\Sigma\rangle)$ is the inverse function of $\langle\Sigma\rangle\tanh(\langle\Sigma\rangle)$. A logarithmic scale is used in the root-mean-square relative fluctuation (ordinate axis) in (a) and (b). (c) Large deviation function of efficiency $J(\eta)$ as a function of stochastic efficiency $\eta$. While the vertical dash-double-dot line patterns (black, red, and blue) represent the values of the stochastic efficiency $\eta$ equivalent to the thermodynamic efficiencies ($\eta_{\rm th}|_{r=0}=0.461$, $\eta_{\rm th}|_{r=0.3}=0.485$, and $\eta_{\rm th}|_{r=0.6}=0.512$), the vertical dash-dotted lines (black, red, and blue) indicate the values of the stochastic efficiency $\eta$ corresponding to the generalized Carnot efficiencies ($\eta_C^{\rm gen}|_{r=0}=0.778$, $\eta_C^{\rm gen}|_{r=0.3}=0.817$, and $\eta_C^{\rm gen}|_{r=0.6}=0.884$). In (a), $\tau_h=0.5$, in (b), $\tau_{\rm dri}=0.0005$, and in (c), $\tau_{\rm dri}=0.001$ and $\tau_h=5$. The other parameters are same as in Fig. 2.

The root-mean-square relative fluctuation of power $\sqrt{\delta P^2}/P$ is equivalent to the coefficient of variation of the work $\sqrt{\delta {\rm w}_{\rm tot}^2}/\langle {\rm w}_{\rm tot}\rangle$. It measures the dispersion of the probability distribution and thus describes the machine stability. The relative power fluctuation decreases quickly as squeezing parameter $r$ increases, as shown in Figs. 4(a) and 4(b). Note that the total stochastic entropy production $\Sigma$, $\Sigma(q_h,{\rm w}_{\rm tot})=(\beta_c-\beta_h^{\rm eff})q_h+\beta_c{\rm w}_{\rm tot}$, is distributed according to the probability distribution $p(\Sigma)$. This distribution and its counterpart for the time-reversed cycle [the clockwise direction in Fig. 1(a)] satisfy the fluctuation theorems $p(\Sigma)=p_R(-\Sigma)e^{\Sigma}$ [56]. These theorems always imply the generalized thermodynamic uncertainty relation for the stochastic work of the form $\delta {\rm w}_{\rm tot}^2/\langle {\rm w}_{\rm tot}\rangle^2\geqslant {\rm csch}^2[f(\langle\Sigma\rangle)]$ [57,58], where $f(x)$ is the inverse function of $x\tanh(x)$. The coefficient of variation of power is therefore bounded by $\sqrt{\delta P^2}/P\geqslant {\rm csch}[f(\langle\Sigma\rangle)]$, with the total entropy production $\langle\Sigma\rangle=-(\beta_c\langle q_c\rangle+\beta_h^{\rm eff}\langle q_h\rangle)$, as can been seen from Fig. 4(a). Figure 4(b) shows that the oscillation time scale of power fluctuation with respect to the thermal-contact time $\tau_h$ agrees with the corresponding power and efficiency in Fig. 3(b). The relative power fluctuation $\sqrt{\delta P^2}/P$ decreases while thermal-contact time $\tau_h$ or driving time $\tau_{\rm dri}$ increases. In physical terms, the larger the thermal-contact time or driving time (quick driving accounting for quantum coherence), the closer the system to the stationary state, so the nonequilibrium thermal fluctuation of the power is expected to decrease.

We plot the large deviation function of stochastic efficiency in Fig. 4(c), where the curve has a maximum when the stochastic efficiency $\eta=\eta_C^{\rm gen}$ ($\eta_C^{\rm gen}$ reduces to the Carnot efficiency $\eta_C=1-\beta_h/\beta_c$ if $r=0$) and a minimum at $\eta=\eta_{\rm th}$. Since the work and heat are fluctuating quantities, the negative values of the stochastic efficiency $\eta$, with $\eta={\rm w}_{\rm tot}/q_h$, occur when the heat $q_h$ is positive with negative work ${\rm w}_{\rm tot}$ or vice versa, and the values of the efficiency $>1$ happen when the heat $q_c$ is positive. The function $J(\eta)$ is situated between a maximum at the generalized Carnot efficiency $\eta_C^{\rm gen}$ and a minimum at the thermodynamic efficiency $\eta_{\rm th}$, which recovers the case of no squeezing [65,67]. We find that the standard thermodynamic efficiency is the most likely value, and the generalized Carnot efficiency is the least likely. Furthermore, the rate function $J(\eta)$ is strictly larger in the presence of squeezing than the case without squeezing, with the exception of the point $\eta=\eta_{\rm th}$. Figure 4(c) shows that the convergence of the heat engine toward the thermodynamic efficiency is improved by including the reservoir squeezing. This may be understood by noting that quantum efficiency fluctuations,

which can be related to machine stability, are suppressed under reservoir squeezing.

## VI. DISCUSSIONS AND CONCLUSIONS

Experimentally, a quantum Otto engine alternatively driven by a thermal and a squeezed bath can be implemented by employing the spin of the valence electron pertaining to a single trapped $^{40}Ca^{+}$ ion [84,85] confined in a Paul trap. As the magnetic field along the $z$ direction yields a Zeeman splitting, the Hamiltonian of the spin system can be given by $H = \hbar\omega_z\sigma_z/2$. The coupling between the spin and harmonic motion is mediated via an optical standing wave by a spin-dependent optical dipole force along the oscillation ($x$) direction, which reads $\hbar\Delta_{\rm sw}\sin(k_{\rm sw}\hat{x})\sigma_z/2$, with the amplitude of the standing wave $\Delta_{\rm sw}$ and effective wave number $k_{\rm sw}$. The unharmonic term $\hbar\Delta_{\rm sw}\sin(k_{\rm sw}\hat{x})\sigma_z/2$ will be responsible for realization of the squeezed state of the motion [85,86]. The machine performance can be observed when choosing experimental parameters, which confirms our theoretical prediction based on the choice of values for $\omega_c$ and $\omega_h$ falling into a relatively large range (see Appendix D).

The efficiency at maximum power, the focus of field of finite-time thermodynamics, is the quantity of great interest for practical applications. Under an endoreversible condition [87], where the irreversibility originates exclusively from the thermal-contact processes due to finite heat currents, both unitary strokes satisfy the quantum adiabatic condition, and thus, the parameters $\xi$ and $\zeta_{hc,ch}$ are vanishing. In such a case, the dynamics of the system along the hot isochore with $t_1 \leqslant t \leqslant t_2$ and the cold isochore with $t_3 \leqslant t \leqslant t_3 + \tau_c$, Eqs. (2) and (7), takes the form:

$$\begin{pmatrix} \dot{p}_t^e & 0 \\ 0 & \dot{p}_t^g \end{pmatrix} = \Gamma_\alpha^- \begin{pmatrix} -p_t^e & 0 \\ 0 & p_t^e \end{pmatrix} + \Gamma_\alpha^+ \begin{pmatrix} p_t^g & 0 \\ 0 & -p_t^g \end{pmatrix}, \quad (23)$$

where the subscripts $\alpha = h, c$ correspond to the hot and cold isohoric strokes, respectively. Here, $\Gamma_h^+ = \gamma_h N_h^{\rm ss}$ and $\Gamma_h^- = \gamma_h(1 + N_h^{\rm ss})$, with $N_h^{\rm ss}$ defined in Eq. (3); $\Gamma_c^+ = \gamma_h N_c^{\rm th}$ and $\Gamma_c^- = \gamma_h(1 + N_c^{\rm th})$, with $N_c^{\rm th} = [\exp(\beta_h\hbar\omega_h) - 1]^{-1}$. Based on Eq. (23), we obtain the explicit expressions of the power as a function of the time allocations to the four processes and then maximize the power in the two consecutive steps, showing that the expression for the efficiency at maximum power [33,34] $\eta_{mp} = 1 - \sqrt{\mathrm{sech}(2r)\beta_h/\beta_c}$ is reproduced in the high-temperature limit (see Appendix C for more details).

A natural extension of our approach allows us to discuss another quantum engine model that works with a harmonic system. Unlike the case in our previous model, where the working substance is a two-level system, in the present machine, there are many energy levels for the harmonic system. In the case when a harmonic system with constant Hamiltonian $H$ is weakly coupled to a heat reservoir, we start our analysis by using Eq. (1), $\frac{d\rho}{dt} = -\frac{i}{\hbar}[H, \rho_t] + \mathcal{L}_D(\rho_t)$. Since we cannot directly determine the time-dependent density matrix as we did for the spin system, we determine the expectation value of an operator $\hat{X}$ which is not explicitly time dependent by using the Lindblad equation, which reads

$$\frac{d\langle\hat{X}\rangle}{dt} = -\frac{i}{\hbar}\langle[H, \hat{X}]\rangle + \mathrm{Tr}[\hat{X}\mathcal{L}_D(\rho_t)]. \quad (24)$$

Here, the dissipation term $\mathcal{L}_D(\rho_t)$ can be written in terms of annihilation and creation operators ($\hat{a}$ and $\hat{a}^\dagger$) [75]:

$$\mathcal{L}_D(\rho_t) = \gamma(\bar{n}+1)\big[\hat{a}\rho_t\hat{a}^\dagger - \tfrac{1}{2}\{\hat{a}^\dagger\hat{a}, \rho_t\}\big] + \gamma\bar{n}\big[\hat{a}^\dagger\rho_t\hat{a} - \tfrac{1}{2}\{\hat{a}\hat{a}^\dagger, \rho_t\}\big]. \quad (25)$$

If the reservoir is squeezed, $\hat{a}$ ($\hat{a}^\dagger$) in Eq. (25) is replaced by $\hat{a}_s$ ($\hat{a}_s^\dagger$), with $\hat{a}_s = \hat{a}\cosh(r) + \hat{a}^\dagger\sinh(r)$ [75], leading to $\mathcal{L}_D(\rho_t) = \gamma(\bar{n}+1)[\hat{a}_s\rho_t\hat{a}_s^\dagger - \frac{1}{2}\{\hat{a}_s^\dagger\rho_t\hat{a}_s, \rho_t\}] + \gamma\bar{n}[\hat{a}_s^\dagger\rho_t\hat{a}_s - \frac{1}{2}\{\hat{a}_s\hat{a}_s^\dagger\rho_t\}]$. To describe the instantaneous state of the harmonic oscillator, we introduce three operators: the Hamiltonian $H = \frac{1}{2m}\mathcal{P}^2 + \frac{m}{2}\omega^2 Q$, the Lagrangian $L = \frac{1}{2m}\mathcal{P}^2 - \frac{m}{2}\omega^2 Q$, and the position momentum correlation $\mathcal{C} = \frac{1}{2}\omega(Q\mathcal{P} + \mathcal{P}Q)$. These operators are given by $H = \frac{1}{2}\hbar\omega(\hat{a}\hat{a}^\dagger + \hat{a}^\dagger\hat{a}), L = -\frac{\hbar\omega}{2}(\hat{a}^2 + \hat{a}^{\dagger 2})$, and $\mathcal{C} = -i\frac{\hbar\omega}{2}(\hat{a}^2 - \hat{a}^{\dagger 2})$, respectively. With these, we can obtain the resulting finite-time performance and fluctuations in the harmonic quantum engines, demonstrating that the findings from the two-level heat engines can be translated into the harmonic thermal machines (see Appendix E).

In summary, we have presented a unified thermodynamic theory for a squeezed-bath-driven quantum Otto engine whereby all the variables are periodic and the efficiency is irrelevant to the Carnot value. We have shown that the engine under squeezing can outperform its nonsqueezing counterpart by dramatically enhancing efficiency and power output and even that the efficiency at positive power may beat the quantum Otto limit. We have demonstrated that reservoir squeezing significantly decreases relative power fluctuations and leads to faster convergence of the machine efficiency to its most probable value. Our findings demonstrate the potential of quantum engines fueled by nonthermal reservoirs [88] to realize ideal nanoscale engines with more efficient, larger power, and higher stability.

## ACKNOWLEDGMENTS

This work was supported by NSFC under Grants No. 11875034, No. 12174461, No. 12234012, No. 12334012, and No. 52327808. J.H W. also acknowledges support from the Major Program of Jiangxi Provincial Natural Science Foundation under Grant No. 20224ACB201007 and the Opening Project of Shanghai Key Laboratory of Special Artificial Microstructure. W.-M.L. also acknowledges support from National Key R&D Program of China under Grants No. 2021YFA1400900, No. 2021YFA0718300, and No. 2021YFA1402100, and Space Application System of China Manned Space Program.

## APPENDIX A: AVERAGE WORK AND WORK FLUCTUATIONS

The joint distribution of quantum work $\mathrm{w_{tot}}$ and heat $q_h$ determines the distribution functions of work and heat, respectively. For the two-level system, the ground and excited eigenenergies are $\varepsilon_g^\alpha = -\hbar\omega_\alpha$ and $\varepsilon_e^\alpha = \hbar\omega_\alpha$, where $\alpha = c, h$ correspond to the cold and hot isochores, respectively. Let $\xi \equiv |\langle n(t_0)|U_{ch}|m(t_1)\rangle|^2 = |\langle i(t_2)|U_{hc}|j(t_3)\rangle|^2 (m, n, i, j = e, g)$ [1] be the level transition probability during expansion or compression for the two level system. When the unitary driven

stroke is not slow, $\xi$ is positive due to the population exchange between the levels, but it would be vanishing when the unitary stroke proceeds slowly enough for the quantum adiabatic condition to be satisfied. Using Eq. (14), the probability distributions of work and heat can be calculated as

$$
\begin{aligned}
p(\mathrm{w}_{\mathrm{tot}}) &= \int dq_h p(\mathrm{w}_{\mathrm{tot}}, q_h) \\
&= \left[p^e_{t_0}p^e_{t_2} + p^g_{t_0}p^g_{t_2} - 2\left(p^e_{t_0}p^e_{t_2} + p^g_{t_0}p^g_{t_2}\right)\xi + \xi^2\right]\delta(\mathrm{w}_{\mathrm{tot}}) + 2\zeta_{hc}\left(\xi - p^g_{t_0}\right)\delta\left(\mathrm{w}_{\mathrm{tot}} + \frac{\hbar\omega_h}{2}\right) \\
&\quad + p^e_{t_0}p^e_{t_2}\xi^2\delta(\mathrm{w}_{\mathrm{tot}} + \hbar\omega_c + \hbar\omega_h) + p^g_{t_0}(1-\xi)\xi\delta(\mathrm{w}_{\mathrm{tot}} - \hbar\omega_c) + 2p^g_{t_0}\zeta_{hc}(1-\xi)\delta\left(\mathrm{w}_{\mathrm{tot}} - \hbar\omega_c + \frac{\hbar\omega_h}{2}\right) \\
&\quad + p^e_{t_2}(1-\xi)\xi\delta(\mathrm{w}_{\mathrm{tot}} + \hbar\omega_h) + p^g_{t_0}p^e_{t_2}(1-\xi)^2\delta(\mathrm{w}_{\mathrm{tot}} - \hbar\omega_c + \hbar\omega_h) + 2\zeta_{ch}\left(\xi - p^g_{t_2}\right)\delta\left(\mathrm{w}_{\mathrm{tot}} + \frac{\hbar\omega_c}{2}\right) \\
&\quad + 4\zeta_{ch}\zeta_{hc}\delta\left(\mathrm{w}_{\mathrm{tot}} + \frac{\hbar\omega_c + \hbar\omega_h}{2}\right) + 2\zeta_{ch}\left(p^e_{t_2} - \xi\right)\delta\left(\mathrm{w}_{\mathrm{tot}} - \frac{\hbar\omega_c}{2}\right) - 4\zeta_{ch}\zeta_{hc}\delta\left(\mathrm{w}_{\mathrm{tot}} - \frac{\hbar\omega_c - \hbar\omega_h}{2}\right) \\
&\quad - 2p^e_{t_2}\zeta_{ch}\xi\delta\left(\mathrm{w}_{\mathrm{tot}} + \frac{\hbar\omega_c}{2} + \hbar\omega_h\right) + 2p^e_{t_2}\zeta_{ch}(\xi-1)\delta\left(\mathrm{w}_{\mathrm{tot}} - \frac{\hbar\omega_c}{2} + \hbar\omega_h\right) + p^g_{t_2}(1-\xi)\xi\delta(\mathrm{w}_{\mathrm{tot}} - \hbar\omega_h) \\
&\quad + 2\zeta_{hc}\left(p^e_{t_0} - \xi\right)\delta\left(\mathrm{w}_{\mathrm{tot}} - \frac{\hbar\omega_h}{2}\right) + p^g_{t_0}p^g_{t_2}\xi^2\delta(\mathrm{w}_{\mathrm{tot}} - \hbar\omega_c - \hbar\omega_h) + 2p^g_{t_0}\zeta_{hc}\xi\delta\left(\mathrm{w}_{\mathrm{tot}} - \hbar\omega_c - \frac{\hbar\omega_h}{2}\right) \\
&\quad + 2p^g_{t_2}\zeta_{ch}(1-\xi)\delta\left(\mathrm{w}_{\mathrm{tot}} - \hbar\omega_h + \frac{\hbar\omega_c}{2}\right) - 4\zeta_{ch}\zeta_{hc}\delta\left(\mathrm{w}_{\mathrm{tot}} - \frac{\hbar\omega_h - \hbar\omega_c}{2}\right) + 2p^g_{t_2}\zeta_{ch}\xi\delta\left(\mathrm{w}_{\mathrm{tot}} - \frac{\hbar\omega_c}{2} - \hbar\omega_h\right) \\
&\quad + 4\zeta_{ch}\zeta_{hc}\delta\left(\mathrm{w}_{\mathrm{tot}} - \frac{\hbar\omega_c + \hbar\omega_h}{2}\right) + p^e_{t_0}(1-\xi)\xi\delta(\mathrm{w}_{\mathrm{tot}} + \hbar\omega_c) - 2p^e_{t_0}\zeta_{hc}\xi\delta\left(\mathrm{w}_{\mathrm{tot}} + \hbar\omega_c + \frac{\hbar\omega_h}{2}\right) \\
&\quad + p^e_{t_0}p^g_{t_2}(1-\xi)^2\delta(\mathrm{w}_{\mathrm{tot}} - \hbar\omega_h + \hbar\omega_c) + 2p^e_{t_0}\zeta_{hc}(\xi-1)\delta\left(\mathrm{w}_{\mathrm{tot}} - \frac{\hbar\omega_h}{2} + \hbar\omega_c\right),
\end{aligned}
\tag{A1}
$$

and

$$
\begin{aligned}
p(q_h) &= \int d\mathrm{w}_{\mathrm{tot}} p(\mathrm{w}_{\mathrm{tot}}, q_h) \\
&= \left\{\left[p^g_{t_0}(1-\xi) + p^e_{t_0}\xi - 2\zeta_{ch}\right]p^g_{t_2} + \left[p^e_{t_0}(1-\xi) + p^g_{t_0}\xi + 2\zeta_{ch}\right]p^e_{t_2}\right\}\delta(q_h) \\
&\quad + \left[p^g_{t_0}(1-\xi) + p^e_{t_0}\xi - 2\zeta_{ch}\right]p^e_{t_2}\delta(q_h - \hbar\omega_h) + \left[p^e_1(1-\xi) + p^g_{t_0}\xi + 2\zeta_{ch}\right]p^g_{t_2}\delta(q_h + \hbar\omega_h).
\end{aligned}
\tag{A2}
$$

In deriving these, we have used $p^g_{t_0} = \langle g(t_0)|\rho_{t_0}|g(t_0)\rangle$, $p^e_{t_0} = \langle e(t_0)|\rho_{t_0}|e(t_0)\rangle$, $p^g_{t_2} = \langle g(t_2)|\rho_{t_2}|g(t_2)\rangle$, $p^e_{t_2} = \langle e(t_2)|\rho_{t_2}|e(t_2)\rangle$, $\zeta_{ch} = -\mathrm{Re}[U^{gg}_{ch}\langle g(t_0)|\rho_{t_0}|e(t_0)\rangle U^{eg\dagger}_{ch}]$, and $\zeta_{hc} = -\mathrm{Re}[U^{gg}_{hc}\langle g(t_2)|\rho_{t_2}|e(t_2)\rangle U^{eg\dagger}_{hc}]$. Integrating over the probability distribution function Eq. (A1) allows us to find the expressions for the first two central moments of quantum work. The average work Eq. (1) is derived as

$$
\begin{aligned}
-\langle \mathrm{w}_{\mathrm{tot}}\rangle &= -\int d\mathrm{w}_{\mathrm{tot}} p(\mathrm{w}_{\mathrm{tot}})\mathrm{w}_{\mathrm{tot}} \\
&= \hbar(\omega_h - \omega_c)\left(p^g_{t_0}p^e_{t_2} - p^e_{t_0}p^g_{t_2}\right) - 2\hbar\omega_h\zeta_{ch} - 2\hbar\omega_c\zeta_{hc} - \left[\hbar(\omega_c - \omega_h)\left(p^e_{t_0}p^g_{t_2} - p^g_{t_0}p^e_{t_2}\right) + \hbar(\omega_c + \omega_h)\left(p^g_{t_0}p^g_{t_2} - p^e_{t_0}p^e_{t_2}\right)\right]\xi \\
&= \hbar(\omega_h - \omega_c)(\langle n_{t_2}\rangle - \langle n_{t_0}\rangle) + 2\hbar\xi(\omega_c\langle n_{t_2}\rangle + \omega_h\langle n_{t_0}\rangle) - 2\hbar\omega_h\zeta_{ch} - 2\hbar\omega_c\zeta_{hc} \\
&= \langle \mathrm{w}_{\mathrm{trls}}\rangle + \langle \mathrm{w}_{\mathrm{coh}}\rangle + \langle \mathrm{w}_{\mathrm{fri}}\rangle,
\end{aligned}
\tag{A3}
$$

where $\langle \mathrm{w}_{\mathrm{trls}}\rangle = \hbar(\omega_h - \omega_c)(\langle n_{t_2}\rangle - \langle n_{t_0}\rangle)$, $\langle \mathrm{w}_{\mathrm{coh}}\rangle = -2\hbar\omega_h\zeta_{ch} - 2\hbar\omega_c\zeta_{hc}$, and $\langle \mathrm{w}_{\mathrm{fri}}\rangle = 2\hbar\xi(\omega_c\langle n_{t_2}\rangle + \omega_h\langle n_{t_0}\rangle)$ correspond to the transitionless work, coherent work, and frictional work, respectively. The work fluctuations are obtained as

$$
\begin{aligned}
\langle \mathrm{w}^2_{\mathrm{tot}}\rangle &= \int d\mathrm{w}_{\mathrm{tot}} p(\mathrm{w}_{\mathrm{tot}})\mathrm{w}^2_{\mathrm{tot}} \\
&= \hbar^2\omega_c^2\left[p^g_{t_0}p^e_{t_2} + p^e_{t_0}p^g_{t_2} + \left(p^e_{t_0} - p^g_{t_0}\right)\left(p^e_{t_2} - p^g_{t_2}\right)\xi - 2\left(p^e_{t_0} - p^g_{t_0}\right)\zeta_{hc}\right] \\
&\quad + \hbar^2\omega_h^2\left[p^g_{t_0}p^e_{t_2} + p^e_{t_0}p^g_{t_2} + \left(p^e_{t_0} - p^g_{t_0}\right)\left(p^e_{t_2} - p^g_{t_2}\right)\xi - 2\left(p^e_{t_2} - p^g_{t_2}\right)\zeta_{ch}\right] + \hbar^2\omega_h\omega_c\left[2\left(p^g_{t_0}p^e_{t_2} + p^e_{t_0}p^g_{t_2}\right)(2\xi - 1)\right. \\
&\quad \left. + 2\left(p^e_{t_0} - p^g_{t_0}\right)\left(p^e_{t_2} - p^g_{t_2}\right)\xi^2 + 2\zeta_{hc}\left(p^e_{t_0} - p^g_{t_0}\right) + 2\zeta_{ch}\left(p^e_{t_2} - p^g_{t_2}\right) - 4\zeta_{hc}\xi\left(p^e_{t_0} - p^g_{t_0}\right) - 4\zeta_{ch}\xi\left(p^e_{t_2} - p^g_{t_2}\right) + 8\zeta_{ch}\zeta_{hc}\right] \\
&= \omega_h^2\left[\frac{1}{2} - 2\langle n_{t_2}\rangle(\langle n_{t_0}\rangle + 2\zeta_{ch} - 2\langle n_{t_0}\rangle\xi)\right] + \omega_c^2\left[\frac{1}{2} - 2\langle n_{t_0}\rangle(\langle n_{t_2}\rangle + 2\zeta_{hc} - 2\langle n_{t_2}\rangle\xi)\right] \\
&\quad + \omega_c\omega_h\left[2\xi - 1 + 4\zeta_{ch}\langle n_{t_2}\rangle(1-2\xi) + 4\zeta_{hc}\langle n_{t_0}\rangle(1-2\xi) + 4\langle n_{t_0}\rangle\langle n_{t_2}\rangle(2\xi^2 + 1 - 2\xi) + 8\zeta_{ch}\zeta_{hc}\right].
\end{aligned}
\tag{A4}
$$

In deriving Eqs. (A3) and (A4), we have used $\langle n_{t_0}\rangle = (p^e_{t_0} - p^g_{t_0})/2$ and $\langle n_{t_2}\rangle = (p^e_{t_2} - p^g_{t_2})/2$, which are average populations of the system at time $t = t_0$ and $t = t_2$, respectively. By very simple algebra, we use Eq. (A2) to obtain the macroscopic heat injection $\langle q_h\rangle = \int dq_h q_h p(q_h) = \hbar\omega_h[p^g_{t_0}p^e_{t_2} - p^e_{t_0}p^g_{t_2} + (p^e_{t_0} - p^g_{t_0})\xi - 2\zeta_{ch}]$, which in terms of the populations $\langle n_{t_0}\rangle$ and $\langle n_{t_2}\rangle$, can be re-expressed by Eq. (16). By combining Eqs. (A3) and (A4), we can obtain the work fluctuations, $\delta \mathrm{w}^2 = \langle \mathrm{w}^2\rangle - \langle \mathrm{w}\rangle^2$ [cf. Eq. (17)].

## APPENDIX B: CARNOT-UNIVERSAL THERMODYNAMIC BOUND FOR THE ENGINE FOLLOWING FROM ANOTHER DEFINITION OF THE EFFICIENCY

For quantum heat engines driven by nonthermal reservoirs, the additional energetic cost necessary to maintain the non-Gibbsian state may be considered. The definition of heat should be modified to account for the additional energy which is responsible for maintaining a squeezed, nonequilibrium steady state, thereby implying that the definition of the efficiency could be modified.

We start our analysis with the total entropy production for a system with Hamiltonian $H$ weakly coupled to a single thermal reservoir of constant inverse temperature $\beta$ with $\beta = 1/(k_B T)$, which was discussed in Sec. III A. For a given external control parameter, the system would reach thermal equilibrium state $\rho^{\mathrm{eq}}_t = e^{-\beta H}/Z$, with the partition function $Z = \mathrm{Tr}(e^{-\beta H})$, provided that the time duration is much larger than the relaxation time. From Eq. (18), the total entropy production is given by $\langle\Sigma\rangle = S - \Psi$, and the differential form of this relation reads

$$\langle \delta\Sigma\rangle = dS - d\Psi \geqslant 0. \tag{B1}$$

By using $\dot{\Psi} = -\mathrm{Tr}(\dot{\rho}_t \ln \rho^{\mathrm{eq}}_t)$, we find that the infinitesimal change of entropy flow is

$$d\Psi = -\mathrm{Tr}\big(\delta\rho_t \ln \rho^{\mathrm{eq}}_t\big) = \beta d(E - F), \tag{B2}$$

where $E = \mathrm{Tr}(\rho H)$ is the internal energy of the system, and $F = -T\ln Z$ is the free energy. Since the infinitesimal change in internal energy of the system $dE$ reads

$$dE = \langle \delta \mathrm{w}\rangle + \langle \delta q\rangle = \mathrm{Tr}(\rho\delta H) + \mathrm{Tr}(H\delta\rho), \tag{B3}$$

where $\langle \delta \mathrm{w}\rangle = \mathrm{Tr}(\rho\delta H)$ and $\langle \delta q\rangle = \mathrm{Tr}(H\delta\rho)$, Eq. (B2) can be written as

$$d\Psi = \mathrm{Tr}(\delta\rho H) = \beta\langle \delta q\rangle. \tag{B4}$$

This holds in the reversible and irreversible processes, in contrast to $\langle dS\rangle \geqslant \beta\mathrm{Tr}(H\delta\rho)$, in which equality is adopted only in the reversible case [71]. Substitution of Eq. (B2) into Eq. (B1) gives rise to

$$\langle \delta\Sigma\rangle = dS - \beta d(E - F) = dS - \beta\langle \delta q\rangle. \tag{B5}$$

If the reservoir is nonthermal due to quintessential quantum effects, such as the squeezing under consideration, the system can only reach the nonequlibrium steady state in the long time limit. As in the classical systems, the total heat for an open system is divided into two parts [52,89–91]: One part is called housekeeping heat responsible for maintaining a nonequilibrium steady state; the other part is an excess heat which is only associated with the entropic cost, namely,

$$\langle q\rangle = \langle q\rangle_{\mathrm{hk}} + \langle q\rangle_{\mathrm{ex}}. \tag{B6}$$

In what follows, we will use $\widetilde{\bullet}$ to denote a physical quantity for the system in contact with the nonthermal reservoir. Accordingly, the first law of thermodynamics can be expressed as

$$d\widetilde{E} = \langle \delta \mathrm{w}\rangle_{\mathrm{ex}} + \langle \delta q\rangle_{\mathrm{ex}}, \tag{B7}$$

where $\widetilde{E}$ is the internal energy for the system, and $\langle \mathrm{w}\rangle_{\mathrm{ex}}$ is the average excess work input. In such a situation, the irreversible entropy production can be obtained via Eq. (18), leading to

$$\delta\widetilde{\Sigma} = d\widetilde{S} - d\widetilde{\Psi}, \tag{B8}$$

where $\widetilde{S} = -\mathrm{Tr}(\widetilde{\rho}_t \ln \widetilde{\rho}_t)$ and $\widetilde{\Psi} = -\mathrm{Tr}(\widetilde{\rho}_t \ln \widetilde{\rho}^{\mathrm{ss}}_t)$, with $\widetilde{\rho}^{\mathrm{ss}}_t$ being the nonequilibrium steady state. As an example, for a spin-$\frac{1}{2}$ system under reservoir squeezing, $\widetilde{\rho}^{\mathrm{ss}}_t$ becomes $\rho^{\mathrm{ss}}_t$, given as the solution of $d\rho^{\mathrm{ss}}_t/dt = \mathcal{L}^{\mathrm{sq}}_{\mathcal{D}}(\rho^{\mathrm{ss}}_t) = 0$, where $\mathcal{L}^{\mathrm{sq}}_{\mathcal{D}}$ was defined by Eq. (2). Considering $\widetilde{E} = \mathrm{Tr}(\widetilde{\rho}H)$, we have

$$\begin{aligned}\widetilde{\Psi} &= -\mathrm{Tr}\big(\widetilde{\rho}_t \ln \widetilde{\rho}^{\mathrm{ss}}_t\big) + \mathrm{Tr}\big(\widetilde{\rho}_t \ln \rho^{\mathrm{eq}}_t\big) - \mathrm{Tr}\big(\widetilde{\rho}_t \ln \rho^{\mathrm{eq}}_t\big)\\ &= -\mathrm{Tr}\big(\widetilde{\rho}_t \ln \rho^{\mathrm{eq}}_t\big) - \big[\mathrm{Tr}\big(\widetilde{\rho}_t \ln \rho^{\mathrm{ss}}_t\big) - \mathrm{Tr}\big(\widetilde{\rho}_t \ln \rho^{\mathrm{eq}}_t\big)\big]\\ &= \beta(\widetilde{E} - \widetilde{F}),\end{aligned} \tag{B9}$$

where we have used $\widetilde{F} = F + T\mathcal{D}(\widetilde{\rho}_t, \widetilde{\rho}^{\mathrm{ss}}_t, \rho^{\mathrm{eq}}_t)$ by introducing $\mathcal{D}(\widetilde{\rho}_t, \widetilde{\rho}^{\mathrm{ss}}_t, \rho^{\mathrm{eq}}_t) \equiv \mathrm{Tr}(\widetilde{\rho}_t \ln \rho^{\mathrm{ss}}_t) - \mathrm{Tr}(\widetilde{\rho}_t \ln \rho^{\mathrm{eq}}_t)$. Interestingly, if the process the system is undergoing is quasistatic with $\widetilde{\rho}_t \to \widetilde{\rho}^{\mathrm{ss}}_t$, the function $\mathcal{D}(\widetilde{\rho}_t, \widetilde{\rho}^{\mathrm{ss}}_t, \rho^{\mathrm{eq}}_t)$ reduces to $D(\widetilde{\rho}^{\mathrm{ss}}_t || \rho^{\mathrm{eq}}_t)$ defined by Eq. (18) as the relative entropy. In such a case, $\widetilde{F}$ becomes the information free energy [92,93]. Using Eq. (B9), we obtain

$$\begin{aligned}d\widetilde{\Psi} &= \beta\mathrm{Tr}(H\delta\rho_t) - \beta[d\widetilde{F} - \mathrm{Tr}(\rho_t\delta H)]\\ &= \beta(\langle \delta q\rangle - \langle \delta q\rangle_{\mathrm{hk}})\\ &= \beta\langle \delta q\rangle_{\mathrm{ex}},\end{aligned} \tag{B10}$$

where we have identified $\langle \delta q\rangle \equiv \mathrm{Tr}(H\delta\rho_t)$ and $\langle \delta q\rangle_{\mathrm{hk}} \equiv d\widetilde{F} - \mathrm{Tr}(\rho_t\delta H)$ as the total heat and housekeeping heat, respectively. This identification confirms the fact that the excess entropy $\widetilde{\Psi}$ is associated with the excess heat $\langle q\rangle_{\mathrm{ex}}$. As emphasized, Eq. (B10) is always valid for an open system evolving in an irreversible or a reversible thermodynamic process.

We now turn to the discussion on the the thermodynamic efficiency for our quantum Otto engine discussed in the main text, by considering the effects of the additional energy cost for creating quantum squeezing on the efficiency. Considering that the thermodynamic entropy $S$ of the system is state dependent, we find that the entropy $S$ must satisfy the relation $S(t) = S(t + \tau_{\mathrm{cyc}})$, with cycle period $\tau_{\mathrm{cyc}}$. That is, the change in the thermodynamic entropy of the system over a cycle is vanishing, yielding the inequality $\langle\Sigma_{\mathrm{tot}}\rangle = -(\widetilde{\Psi}_h + \Psi_c) \geqslant 0$, with $\widetilde{\Psi}_h = \beta_h\langle q_h\rangle_{\mathrm{ex}}$ and $\Psi_c = \beta_c\langle q_c\rangle$, or

$$-\beta_h\langle q_h\rangle_{\mathrm{ex}} - \beta_c\langle q_c\rangle \geqslant 0. \tag{B11}$$

Since no heat is exchanged along the two unitary strokes where the system is isolated from a heat reservoir, the excess work extracted from the system during a cycle $-\langle \mathrm{w}_{\mathrm{tot}}\rangle_{\mathrm{ex}}$ is then given by

$$-\langle \mathrm{w}_{\mathrm{tot}}\rangle_{\mathrm{ex}} = \langle q_h\rangle_{\mathrm{ex}} + \langle q_c\rangle, \tag{B12}$$

with $\langle q_h\rangle_{\rm ex} = \langle q_h\rangle - \langle q_h\rangle_{\rm hk}$. When the machine efficiency is defined as the ratio of the total excess work produced $-\langle {\rm w}_{\rm tot}\rangle_{\rm ex}$ to the excess heat during the hot isochore $\langle q_h\rangle_{\rm ex}$, namely, $\widetilde{\eta} = -\langle {\rm w}_{\rm tot}\rangle_{\rm ex}/\langle q_h\rangle_{\rm ex}$ [71], we can obtain by using Eq. (B12)

$$\widetilde{\eta} = -\frac{\langle {\rm w}_{\rm tot}\rangle_{\rm ex}}{\langle q_h\rangle_{\rm ex}} = 1 + \frac{\langle q_c\rangle}{\langle q_h\rangle_{\rm ex}}. \tag{B13}$$

Combination of Eqs. (B11) and (B13) leads to

$$\widetilde{\eta} \leqslant \eta_C, \tag{B14}$$

with the Carnot efficiency $\eta_C = 1 - \beta_h/\beta_c$. We therefore conclude that, unlike the efficiency given as in Eq. (20) where its upper bound is irrelevant to the Carnot efficiency, the machine efficiency $\widetilde{\eta}$ is bounded by the Carnot limit due to the second law of thermodynamics.

## APPENDIX C: EFFICIENCIES IN SEVERAL SPECIAL CASES

### 1. Efficiencies for large and small differences between two reservoir temperatures

The thermodynamic efficiency, defined by the ratio of the total work to heat injection along the isochore, can be obtained by Eqs. (15) and (16):

$$\eta_{\rm th} = 1 + \frac{\omega_c}{\omega_h}\frac{\langle n_{t_0}\rangle + \langle n_{t_2}\rangle(2\xi - 1) - 2\zeta_{hc}}{\langle n_{t_2}\rangle + \langle n_{t_0}\rangle(2\xi - 1) - 2\zeta_{ch}}. \tag{C1}$$

In the case of the small ratio of the cold bath temperature to the hot bath temperature, $\beta_h\hbar\omega_h \ll \beta_c\hbar\omega_c$, one has $N_h^{\rm ss} \gg N_c^{\rm th}$, where $N_h^{\rm ss}$ and $N_c^{\rm th}$ were defined in Eqs. (3) and (7), respectively. When $N_h^{\rm ss} \gg 1$, $\mathcal{X}$ and $\langle\sigma_z\rangle$ defined in Eq. (4) are particularly small, as both exhibit exponential decay functions of $N_h^{\rm ss}$. The density matrix $\rho_{t_2}$ given by Eq. (4) with $t = t_2$ can thus be approximated by

$$\rho_{t_2} \approx \begin{pmatrix} p_{t_2}^e & 0 \\ 0 & p_{t_2}^g \end{pmatrix}, \tag{C2}$$

where the occupation probability at the excited state $p_{t_2}^e$ is close to that at the ground state $p_{t_2}^g$. This, together with the relation of $\langle n_t\rangle = {\rm Tr}(\rho_t H)/(\hbar\omega)$, implies that the absolute value $|\langle n_{t_2}\rangle|$ should be close to zero. By contrast, as $N_c^{\rm th} \gg N_h^{\rm ss}$, we find that $|\langle n_{t_2}\rangle| \ll |\langle n_{t_0}\rangle|$. We also note that, as the parameter $\zeta_{hc}$ defined in Eq. (A1) is a monotonic increasing function of $\mathcal{X}$, a small $\mathcal{X}$ leads to a negligible parameter $\zeta_{hc}$. As a result, the thermodynamic efficiency in Eq. (C1) can be approximately rewritten as

$$\eta_{\rm th} \approx 1 + \frac{\omega_c}{\omega_h}\frac{\langle n_{t_0}\rangle}{\langle n_{t_0}\rangle(2\xi - 1) - 2\zeta_{ch}}. \tag{C3}$$

Because of the insensitive dependence of the average population $\langle n_{t_0}\rangle$ and the parameter $\xi_{ch}$ [defined in Eq. (A1)] on the squeezing parameter, for the large ratio $\beta_h/\beta_c$, the efficiency tends to be the expression in Eq. (C3), which is independent of the squeezing parameter, as shown in Fig. 5(a).

By contrast, in the linear response regime where the difference between the reservoir temperatures is small, the sensitive dependence of the efficiency on squeezing parameter $r$ is observed in Fig. 5(a). This can be understood by the fact that

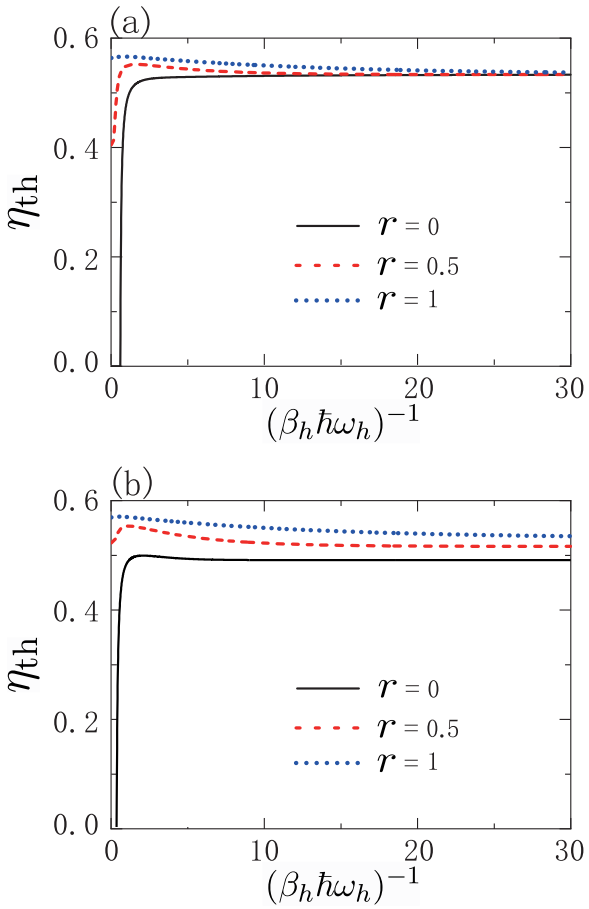


FIG. 5. Efficiency as a function of $(\beta_h\hbar\omega_h)^{-1}$. In (a), $\beta_c = 2/(\hbar\omega_c)$, and in (b), $\beta_c = 4.5\beta_h$. The parameters are $\tau_c = 3$, $\tau_h = 0.2$, and $\tau_{\rm dri} = 0.0005$, $\gamma_c = \gamma_h = 3$.

$\langle n_{t_2}\rangle$ and $\zeta_{hc}$, both of which cannot be neglected in the linear response regime, are strongly dependent on the squeezing parameter.

### 2. Efficiencies at low and high temperatures

We now examine the thermodynamic efficiency in the high- and low-temperature regimes. In the high-temperature limit $\beta_\alpha\hbar\omega_\alpha \ll 1$ ($\alpha = c, h$), we find with $\zeta_{ch} \to 0$ and $\zeta_{hc} \to 0$ that the efficiency in Eq. (C1) becomes

$$\eta_{\rm th}^{\rm high} = 1 + \frac{\omega_c}{\omega_h}\frac{\langle n_{t_0}\rangle + \langle n_{t_2}\rangle(2\xi - 1)}{\langle n_{t_2}\rangle + \langle n_{t_0}\rangle(2\xi - 1)}. \tag{C4}$$

In view of the fact that the derivation of exactly analytical expressions of $\langle n_{t_0}\rangle$ and $\langle n_{t_2}\rangle$ is a formidable task even at high temperatures, we assume the two isochoric processes to be quasistatic to estimate the effects of reservoir squeezing on $\langle n_{t_0}\rangle$ and $\langle n_{t_2}\rangle$. At the quasistatic limit, the mean population $\langle n_{t_0}\rangle$ ($\langle n_{t_2}\rangle$) approaches the value of the thermal (steady) state $\langle n_{t_0}\rangle \to \langle n_c^{\rm eq}\rangle$ ($\langle n_{t_2}\rangle \to \langle n_h^{\rm ss}\rangle$), leading to

$$\eta_{\rm th,quasi}^{\rm high} = 1 + \frac{\omega_c}{\omega_h}\frac{\beta_c\omega_c + {\rm sech}(2r)\beta_h\omega_h(2\xi - 1)}{{\rm sech}(2r)\beta_h\omega_h + \beta_c\omega_c(2\xi - 1)}, \tag{C5}$$

which is thus dependent on squeezing parameter $r$. Beyond the quasistatic limit, where the mean population $\langle n_{t_2}\rangle$,

though not solved analytically, should be dependent on the squeezing parameter $r$, we therefore conclude that the thermodynamic efficiency $\eta_{\rm th}$ is an increasing function of squeezing parameter $r$.

On the other hand, in the low-temperature limit $\beta_\alpha\hbar\omega_\alpha \gg 1$ ($\alpha = c, h$), the quantum coherence related to $\zeta_{ch}$ and $\zeta_{hc}$ cannot be neglected, and the efficiency at low temperatures is still given by Eq. (C1), where the time-dependent functions $\langle n_{t_0}\rangle$ and $\langle n_{t_2}\rangle$ cannot be obtained analytically. As in the high-temperature case, we consider the quasistatic isochores to find an analytical expression for the efficiency in terms of squeezing parameter $r$ in the low-temperature limit where $\tanh(\beta\hbar\omega/2) \approx 1 - 2\exp(-\beta\hbar\omega)$, and the effective inverse temperature in Eq. (6) is approximated by $\beta_h^{\rm eff} \approx \log\{[1 + \sinh^2(r)]/\sinh^2(r)\}/(\hbar\omega_h)$. With consideration of Eq. (C1), we obtain the explicit $r$-dependent expression for the efficiency, which reads

$$\eta_{\rm th,quasi}^{\rm low} = 1 + \frac{\omega_c}{\omega_h}\frac{1 - 2e^{-\beta_c\hbar\omega_c} + [2{\rm sech}^2(r) - 1](2\xi - 1)}{2{\rm sech}^2(r) - 1 + (1 - 2e^{-\beta_c\hbar\omega_c})(2\xi - 1)}. \tag{C6}$$

As emphasized, $\zeta_{hc} \approx 0$ and $\zeta_{ch} \approx 0$ have been used in deriving Eq. (C6). This follows from the fact that the coherence generated in the two unitary strokes should be fully erased after the two quasistatic isochoric processes. Unlike in the high-temperature limit where $\zeta_{ch}$ and $\zeta_{hc}$ become negligible even beyond the quasistatic limit, these two parameters at low temperatures are finite in the finite-time machine operation. Since $\zeta_{ch}$, $\zeta_{ch}$, and $\langle n_{t_2}\rangle$ are dependent on $r$ at low temperatures, we can extend the analytic approximation in Eq. (C6) to the finite-time domain, deducing the dependence of the efficiency on the squeezing at low temperatures.

While our analysis focuses on the quasistatic limit, we illustrate in Fig. 5(b) that the efficiency for the finite-time engine, determined by exactly numerical calculation, is dependent on reservoir squeezing, within the inverse temperature regime ranging from $\beta_h\hbar\omega_h = 0.01$ to $\beta_h\hbar\omega_h = 30$, with $\beta_c = 4.5\beta_h$.

### 3. Efficiency at maximum power in the high-temperature limit

Under the endoreversible condition, according to Eq. (23), the motion of the system along the hot isochore process $\langle\dot{n}_t\rangle = {\rm Tr}(\dot{\rho}_t H_t\rangle/(\hbar\omega_h)$ can be derived as

$$\begin{aligned}\langle\dot{n}_t\rangle &= \frac{\dot{p}_t^e - \dot{p}_t^g}{2} \\ &= -\Gamma_h\big(\langle n_t\rangle - \langle n_h^{\rm ss}\rangle\big),\end{aligned} \tag{C7}$$

where $\Gamma_h = \Gamma_h^+ + \Gamma_h^-$, $\langle n_h^{\rm ss}\rangle = (\Gamma_h^+ - \Gamma_h^-)/[2(\Gamma_h^- + \Gamma_h^+)] = -\tanh(\beta_h^{\rm eff}\hbar\omega_h/2)/2$, with $\beta_h^{\rm eff}$ defined in Eq. (6). By following the same method, we find that the motion of the system during the cold isochoric stroke with $t_3 \leqslant t \leqslant t_3 + \tau_c$ takes the form:

$$\langle\dot{n}_t\rangle = -\Gamma_c\big(\langle n_t\rangle - \langle n_c^{\rm eq}\rangle\big), \tag{C8}$$

where we have used $\Gamma_c = \Gamma_c^+ + \Gamma_c^-$ and $\langle n_c^{\rm eq}\rangle = (\Gamma_c^+ - \Gamma_c^-)/[2(\Gamma_c^- + \Gamma_c^+)] = -\tanh(\beta_c\hbar\omega_c/2)/2$, with $\Gamma_c^+ = \gamma_c N_c^{\rm eq}$ and $\Gamma_c^- = \gamma_c(1 + N_c^{\rm eq})$.

Combining Eqs. (C7) and (C8) and using boundary conditions of $\langle n_{t_1}\rangle = \langle n_{t_0}\rangle$ and $\langle n_{t_3}\rangle = \langle n_{t_2}\rangle$, we have

$$\langle n_{t_2}\rangle = \langle n_h^{\rm ss}\rangle + \big(\langle n_{t_0}\rangle - \langle n_h^{\rm ss}\rangle\big)\exp(-\Gamma_h\tau_h), \tag{C9}$$

$$\langle n_{t_0}\rangle = \langle n_c^{\rm eq}\rangle + \big(\langle n_{t_2}\rangle - \langle n_c^{\rm eq}\rangle\big)\exp(-\Gamma_c\tau_c). \tag{C10}$$

It follows that the total work extracted per cycle and average heat injection along the hot isochore, Eqs. (5) and (6), turn out to be

$$-\langle {\rm w}_{\rm tot}\rangle = \mathcal{G}(\tau_h, \tau_c)\hbar(\omega_h - \omega_c)\big(\langle n_h^{\rm ss}\rangle - \langle n_c^{\rm eq}\rangle\big), \tag{C11}$$

and

$$\langle q_h\rangle = \mathcal{G}(\tau_h, \tau_c)\hbar\omega_h\big(\langle n_h^{\rm ss}\rangle - \langle n_c^{\rm eq}\rangle\big), \tag{C12}$$

respectively, with $\mathcal{G}(\tau_h, \tau_c) = [\exp(\Gamma_h\tau_h) - 1][\exp(\Gamma_c\tau_c) - 1]/[\exp(\Gamma_c\tau_c + \Gamma_h\tau_h) - 1]$. In the endoreversible case, the machine efficiency $\eta_{\rm th} = -\langle {\rm w}_{\rm tot}\rangle/\langle q_h\rangle$ simplifies to the Otto value:

$$\eta_{\rm th} = \eta_{\rm Otto} = 1 - \frac{\omega_c}{\omega_h}. \tag{C13}$$

From Eq. (C11), we find that the power output $P = -\langle {\rm w}_{\rm tot}\rangle/\tau_{\rm cyc}$ is expressed as a product of two functions: $\mathcal{G}(\tau_c, \tau_h)/\tau_{\rm cyc}$, a function of the time variables only, and $\hbar(\omega_h - \omega_c)(\langle n_h^{\rm ss}\rangle - \langle n_c^{\rm eq}\rangle)$, the other one depending only on the external fields. The optimization by maximizing the power output can be present in the two consecutive steps. We firstly maximize the time-dependent function $\mathcal{G}(\tau_c, \tau_h)/\tau_{\rm cyc}$ by setting $\partial[\mathcal{G}(\tau_c, \tau_h)\tau_{\rm cyc}^{-1}]/\partial\tau_c = \partial[\mathcal{G}(\tau_c, \tau_h)\tau_{\rm cyc}^{-1}]/\partial\tau_h = 0$ to determine the optimal protocols of the machine cycle and then consider the optimization on the external constrains of heat engine to obtain maximum power. In the high-temperature limit where $\tanh(\beta\hbar\omega/2) \approx \beta\hbar\omega/2$, we set $\partial\langle {\rm w}_{\rm tot}\rangle/\partial\omega_h = 0$ and $\partial\langle {\rm w}_{\rm tot}\rangle/\partial\omega_c = 0$ to obtain the optimal values of external fields, leading to $\omega_h/\omega_c = \sqrt{\beta_h^{\rm eff}/\beta_c}$. This, together with Eq. (C13) and $\beta_h^{\rm eff} \approx {\rm sech}(2r)\beta_h$ at the high-temperature limit, gives rise to the efficiency at maximum power $\eta_{mp} = 1 - \sqrt{{\rm sech}(2r)\beta_h/\beta_c}$, which reduces to the so-called Curzon-Ahlborn efficiency [87] $\eta_{CA} = 1 - \sqrt{\beta_h/\beta_c}$ in the absence of squeezing.

## APPENDIX D: MACHINE PERFORMANCE BASED ON THE CHOICES OF THEORETICAL EXPERIMENTAL PARAMETERS

### 1. The choice of the values of the parameters in numerical simulation

All the parameters we have adopted in our numerical simulation are dimensionless. When $\xi = |\langle n|U_{ch}|m\rangle|^2 = |\langle i|U_{hc}|j\rangle|^2 (m, n, i, j = e, g)$ is set to be fixed, the unitary transformation operator, defined as $U_{ch} = \mathcal{T}_> \exp\{-\frac{i}{\hbar}\int_{t_0}^{t_1} dt H_{ch}(t)\}$ or $U_{hc} = \mathcal{T}_> \exp\{-\frac{i}{\hbar}\int_{t_2}^{t_3} dt H_{hc}(t)\}$, should change very slightly. The driving time $\tau_{\rm dri} (= t_1 - t_0 = t_3 - t_2)$ decreases as the frequencies $\omega_{c,h}$ since the unitary operators $U_{hc,ch}$ are almost kept constant. When $N_h^{\rm ss}$ and $N_c^{\rm eq}$ are given, the divergence function $D(\rho_{t_2}||\rho_h^{\rm ss})$ $[D(\rho_{t_0}||\rho_c^{\rm eq})]$ that measures the distance between state $\rho_{t_2}$ ($\rho_{t_0}$) and reference state $\rho_h^{\rm ss}$ ($\rho_c^{\rm eq}$) is insensitive to the selection of frequencies $\omega_c$ and $\omega_h$, though its oscillation frequency is determined by $\omega_c$ and $\omega_h$, as shown in Fig. 6. The divergence function

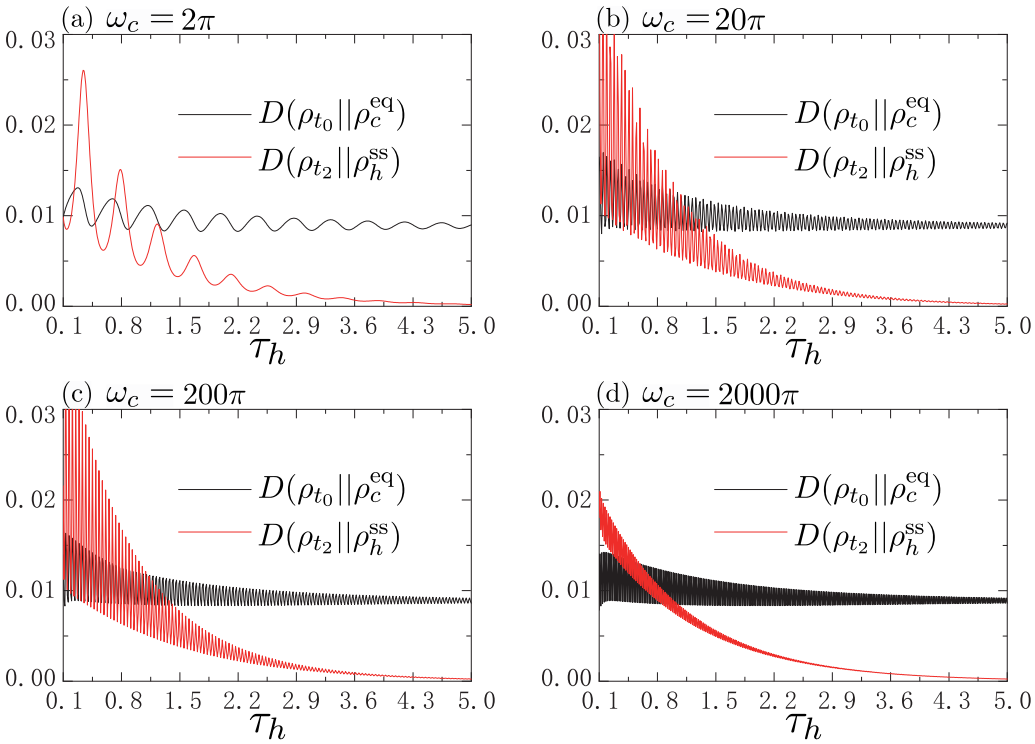


FIG. 6. The Kullback-Leibler-Umegaki divergence $D(\rho_{t_0}||\rho_c^{\rm eq})$ or $D(\rho_{t_0}||\rho_c^{\rm eq})$ as a function of the thermal-contact time $\tau_h$. In (a)–(d), $\omega_c = 2\pi$, $20\pi$, $200\pi$, and $2000\pi$, respectively. For instance, for given $\xi = 0.02318$, these four values correspond to $\tau_{\rm dri} = 0.5$, 0.05, 0.005, and 0.0005, respectively. The other parameters are $\tau_c = 0.5$, $\omega_h = 2.25\omega_c$, $\beta_c = 2/(\hbar\omega_c)$, $\beta_h = 1/(\hbar\omega_h)$, $r = 1$, and $\gamma_c = \gamma_h = 3$.

$D(\rho_{t_2}||\rho_h^{\rm ss})$ is also observed to become vanishing around $\tau_h = 5.0$, at which the system approaches the steady state $\rho_h^{\rm ss}$. This results in the fact that the values of $\omega_{c,h}$ in our numerical simulation have a trivial impact on the thermal contact time $\tau_h$ but an important effect on the driving time $\tau_{\rm dri}$. For instance, if $\omega_c/2\pi = 1$ and $\omega_h = 2.25\omega_c$, with no change in other parameters, the adiabaticity parameter $\xi$ becomes vanishing when $\tau_{\rm dri} \approx 2.5$, which means that the total cycle period $\tau_{cyc}$ is contributed by both thermal-contact and unitary driving times. In such a choice of parameters, except that the power as a function of driving time $\tau_{\rm dri}$ goes from increasing to decreasing [see Fig. 7(a)], the behaviors of the power as

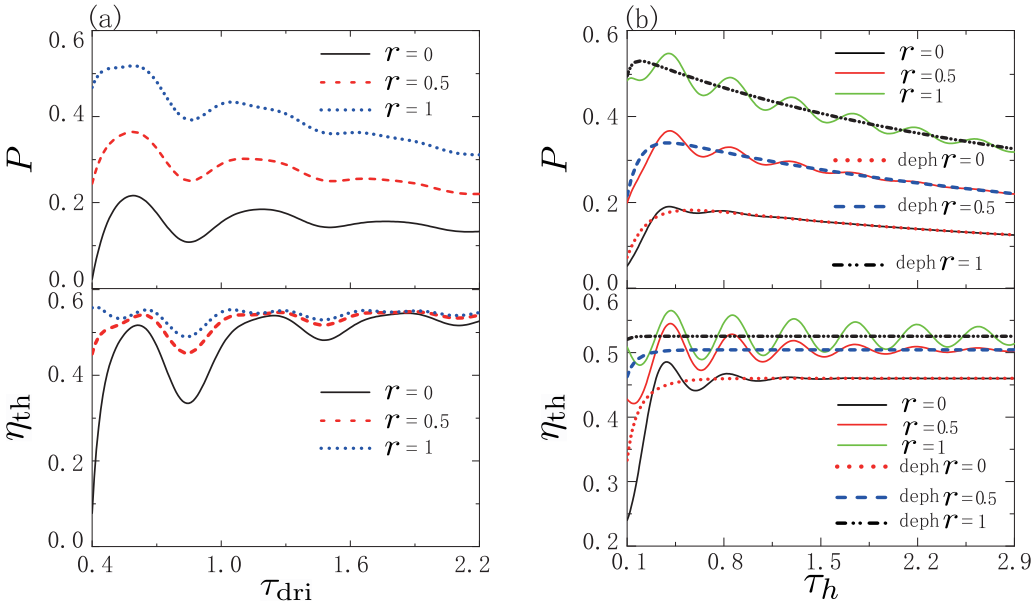


FIG. 7. (a) Power $P$ (up) and thermodynamic efficiency $\eta_{\rm th}$ (bottom) as a function of driving time $\tau_{\rm dri}$, with $\tau_h = 0.5$. (b) Power $P$ (up) and thermodynamic efficiency $\eta_{\rm th}$ (bottom) as a function of thermal-contact time $\tau_h$, with $\tau_{\rm dri} = 0.5$. In (b), the cases of $r = 0$, 0.5, 1 in the dephased engine cycle (labeled deph) are represented by the red dotted line, blue dashed line, and black dash-double-dot line, respectively. The parameters are $\omega_c = 2\pi$, $\omega_h = 2.25\omega_c$, $\beta_c = 2/(\hbar\omega_c)$, $\beta_h = 1/(\hbar\omega_h)$, $\tau_c = 3$, and $\gamma_c = \gamma_h = 3$.

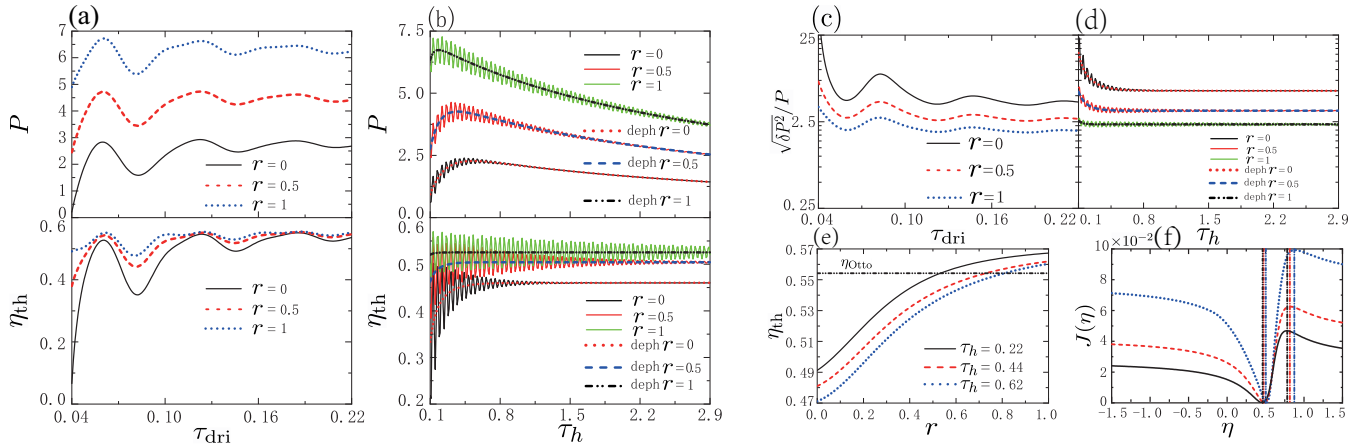


FIG. 8. (a) Power $P$ (up) and thermodynamic efficiency $\eta_{\rm th}$ (bottom) as a function of driving time $\tau_{\rm dri}$. (b) Power $P$ (up) and thermodynamic efficiency $\eta_{\rm th}$ (bottom) as a function of thermal-contact time $\tau_h$. In (b), the cases of $r = 0, 0.5, 1$ in the dephased engine cycle (labeled deph) are represented by the red dotted line, blue dashed line, and black dash-double-dot line, respectively. Root-mean-square relative fluctuation of power $\sqrt{\delta P^2}/P$ as functions of (c) driving time $\tau_{\rm dri}$ and (d) thermalization time $\tau_h$. A logarithmic scale is used in the root-mean-square relative fluctuation (ordinate axis) in (c) and (d). (e) Efficiency as a function of squeezing parameter with given $\tau_h$. (f) Large deviation function of efficiency $J(\eta)$ as a function of stochastic efficiency $\eta$, with $\tau_h = 5$. The vertical dash-double-dot line patterns (black, red, and blue) indicate the values of the stochastic efficiency $\eta$ equal to the thermodynamic efficiencies ($\eta_{\rm th}|_{r=0} = 0.46$, $\eta_{\rm th}|_{r=0.3} = 0.48$, and $\eta_{\rm th}|_{r=0.6} = 0.51$), and the vertical dash-dotted lines (black, red, and blue) represent the quantum efficiencies equivalent to the generalized Carnot values ($\eta_C^{\rm gen}|_{r=0} = 0.78$, $\eta_C^{\rm gen}|_{r=0.3} = 0.82$, and $\eta_C^{\rm gen}|_{r=0.6} = 0.88$). In (a) and (c), $\tau_h = 0.5$, and in (b) and (d)–(f), $\tau_{\rm dri} = 0.05$. The other parameters are $h = 1$, $\omega_c/2\pi = 10$, $\omega_h = 2.25\omega_c$, $\beta_c = 2/(\hbar\omega_c)$, $\beta_h = 1/(\hbar\omega_h)$, $\tau_c = 3$, and $\gamma_c = \gamma_h = 3$.

a function of thermal contact time and the efficiency as a function of $\tau_h$ (or $\tau_{\rm dri}$) in Fig. 7(b) are like those reported in Fig. 3(d). As another example, if we adopt $\omega_c/2\pi = 10$, with $\omega_h = 2.25\omega_c$, all results obtained in the main text would be changed quantitatively but not qualitatively [see, for example, Fig. 8]. Therefore, the selection of values for $\omega_c$ and $\omega_h$ falls into a relatively large range that produces similar results. However, the difference between the scales of driving time and thermal-contact time based on the choice of the values of the frequencies $\omega_{c,h}$ in the main text can be compatible with the realizable experiment in Sec. D 2.

### 2. Power and efficiency based on the choice of the experimental parameters

The Hamiltonian of the harmonic oscillator is $H_{\rm HO} = \hbar\omega_t\hat{n}_t$, with the number operator $\hat{n}_t$ and the trap frequency $\omega_t$ along $x$. Since $\Delta_{\rm sw} \ll \omega_z$, the spin system is adopted as the working substance, and the system with Hamiltonian $H_{\rm HO} + \hbar\Delta_{\rm sw}\sin(k_{\rm sw}\hat{x})\sigma_z/2$ plays the role of the bath which is squeezed due to the presence of the unharmonic term $\hbar\Delta_{\rm sw}\sin(k_{\rm sw}\hat{x})\sigma_z/2$. Because both the direction and value of the Zeeman splitting are determined by the external magnetic field, the compression and expansion can be implemented by changing the magnetic field. In each experimental cycle, the standing wave is switched on (off) at the initial (final) instant of the hot isochoric stroke, and the magnetic field is changed such that the Hamiltonian of the spin system satisfies the form in the main text. For example, the frequencies of the spin system, determined by magnetic field which may be along the $x$ or $z$ direction, vary from $2\pi \times 8$ to $2\pi \times 14.4$ MHz in each cycle. That is, the frequencies for the spin system along the hot and cold isochoric strokes are $\omega_z = 2\pi \times 14.4$ and $\omega_x = 2\pi \times 8$ MHz, respectively. The inverse temperatures of the hot and cold baths, which are associated with the excitation numbers $N_h^{\rm ss}$ and $N_c^{\rm eq}$, are set to be $\beta_h = 8.385 \times 10^{-6}$ and $\beta_c = 6.037 \times 10^{-5}$ $({\rm peV})^{-1}$. By using thermal interaction strengths $\gamma_h = \gamma_c = 1$ MHz, we show how the power and efficiency behave for finite and vanishing squeezing $r$, as shown in Fig. 9. We see that the results of both the power and thermodynamic efficiency based on choice of experimental parameters agree well with corresponding theoretical predictions, supporting an argument in favor of our approach.

## APPENDIX E: THE PERFORMANCE AND FLUCTUATIONS OF FINITE-TIME QUANTUM OTTO ENGINES WORKING WITH A HARMONIC SYSTEM

The instantaneous state can be captured by the set of three operators: the Hamiltonian $H = \frac{1}{2m}\mathcal{P}^2 + \frac{m}{2}\omega^2 Q$, the Lagrangian $L = \frac{1}{2m}\mathcal{P}^2 - \frac{m}{2}\omega^2 Q$, and the position momentum correlation $\mathcal{C} = \frac{1}{2}\omega(Q\mathcal{P} + \mathcal{P}Q)$. These operators can be written in terms of annihilation and creation operators ($\hat{a}$ and $\hat{a}^\dagger$): $H = \frac{1}{2}\hbar\omega(\hat{a}\hat{a}^\dagger + \hat{a}^\dagger\hat{a})$, $L = -\frac{\hbar\omega}{2}(\hat{a}^2 + \hat{a}^{\dagger 2})$ and $\mathcal{C} = -i\frac{\hbar\omega}{2}(\hat{a}^2 - \hat{a}^{\dagger 2})$, respectively. It follows, using Eqs. (24) and (25), that the dissipation term for an operator $\hat{X}$ is

$$\tilde{\mathcal{L}}_D(\hat{X}) = \gamma(\bar{n}+1)\left[\hat{a}^\dagger\hat{X}\hat{a} - \frac{1}{2}\{\hat{a}^\dagger\hat{a}, \hat{X}\}\right] + \gamma\bar{n}\left[\hat{a}\hat{X}\hat{a}^\dagger - \frac{1}{2}\{\hat{a}\hat{a}^\dagger, \hat{X}\}\right]$$
$$= \frac{\gamma}{2}(\bar{n}+1)\{\hat{a}^\dagger[\hat{X}, \hat{a}] + [\hat{a}^\dagger, \hat{X}]\hat{a}\} + \frac{\gamma}{2}\bar{n}\{\hat{a}[\hat{X}, \hat{a}^\dagger] + [\hat{a}, \hat{X}]\hat{a}^\dagger\}. \quad \text{(E1)}$$

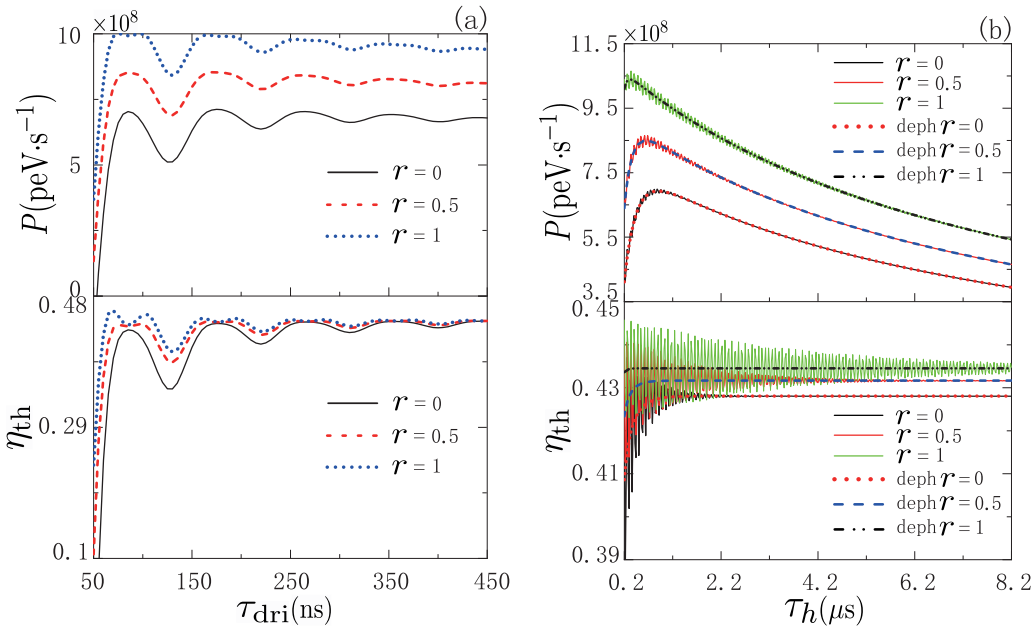


FIG. 9. (a) Power $P$ (up) and thermodynamic efficiency $\eta_{\mathrm{th}}$ (bottom) as a function of driving time $\tau_{\mathrm{dri}}$ in unit of ns. (b) Power $P$ (up) and thermodynamic efficiency $\eta_{\mathrm{th}}$ (bottom) as a function of thermal-contact time $\tau_h$ in units of μs. In (a), $\tau_h = 0.9\,\mu\mathrm{s}$, and in (b), $\tau_{\mathrm{dri}} = 80\,\mathrm{ns}$. In (b), the cases of $r = 0, 0.5,$ and 1 in the dephased engine cycle (labeled deph) are represented by the red dotted line, blue dashed line, and black dot-dashed line, respectively. The other parameters based on the choice of experiment are $\omega_z = 2\pi \times 14.4\,\mathrm{MHz}$, $\omega_x = 2\pi \times 8\,\mathrm{MHz}$, $\gamma_c = \gamma_h = 1\,\mathrm{MHz}$, $\beta_h = 8.385 \times 10^{-6}\,(\mathrm{peV})^{-1}$, $\beta_c = 6.037 \times 10^{-5}\,(\mathrm{peV})^{-1}$, and $\tau_c = 8\,\mu\mathrm{s}$.

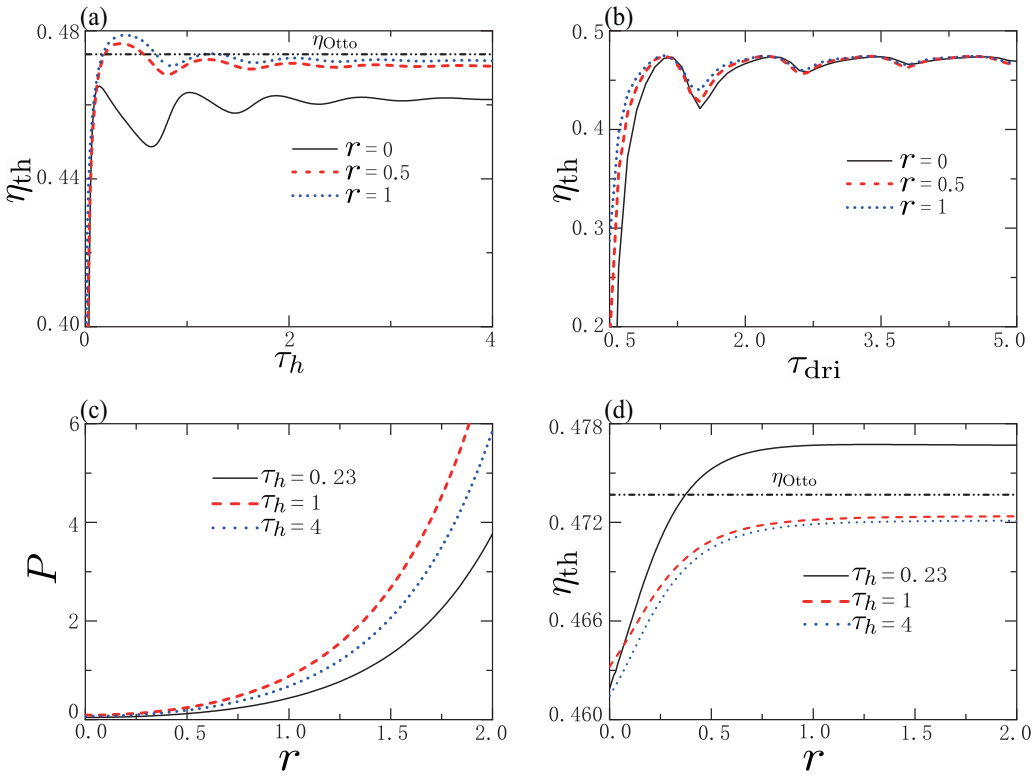


FIG. 10. (a) The thermodynamics efficiency as a function of thermalization time $\tau_h$ for different values of squeezing parameter $r$, with $\tau_{\mathrm{dri}} = 1$. (b) The thermodynamics efficiency as a function of driving time $\tau_{\mathrm{dri}}$ for different values of squeezing parameter $r$, with $\tau_h = 0.6$. (c) The output power and (d) the thermodynamics efficiency as a function of squeezing parameter $r$ for different values of thermalization $\tau_h$, with $\tau_{\mathrm{dri}} = 1$. The parameters are $\hbar = 1$, $\omega_c = 2$, $\omega_h = 3.8$, $\beta_c = 0.6$, $\beta_h = 0.2$, $\tau_c = 1$, and $\gamma_c = \gamma_h = 1$.

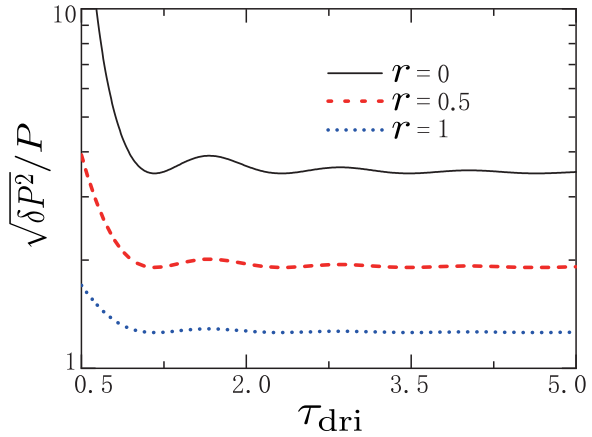


FIG. 11. The root-mean-square relative fluctuation of power as a function of driving time $\tau_{\rm dri}$ for different values of squeezing parameter $r$, with $\tau_h = \tau_c = 4$. The ordinate axis is logarithmically spaced. Same parameters as in Fig. 10.

This implies Heisenberg equation $\frac{d\hat{X}}{dt} = -\frac{i}{\hbar}[H, \hat{X}] + \tilde{\mathcal{L}}_D(\hat{X})$. The set of operators $(H, L, \mathcal{C}, I)^T$, where $I$ is the identity operator and the superscript $T$ stands for transpose of the matrix, determines the state of the harmonic system. Notice that, in the unitary stroke, $\tilde{\mathcal{L}}_D(\hat{X})$ is vanishing. By substituting $\hat{X} \equiv (H, L, \mathcal{C}, I)^T$ into the Heisenberg equation, we can numerically obtain the time-dependent set of operators $\hat{X}$, which reaches a periodic state in each cycle [i.e., $\hat{X}(t) = \hat{X}(t + \tau_{\rm cyc})$], with the cycle period $\tau_{\rm cyc} = \tau_h + \tau_c + 2\tau_{\rm dri}$. We therefore obtain the thermodynamic quantities, such as average work output $-\langle \mathrm{w}_{\rm tot}\rangle = \langle H_{t_0}\rangle - \langle H_{t_1}\rangle + \langle H_{t_3}\rangle - \langle H_{t_2}\rangle$ and average heat injection $\langle q_h\rangle = \langle H_{t_2}\rangle - \langle H_{t_1}\rangle$, where $\langle H_{t_i}\rangle$ denotes the expectation of system Hamiltonian at time $t = t_i (i = 0, 1, 2, 3)$, with $t_i$ being sketched in Fig. 1.

Using the same approach as adopted in the main text, we can determine the machine performance parameters such as the average power $P = -\langle \mathrm{w}_{\rm tot}\rangle/\tau_{\rm cyc}$ and thermodynamic efficiency $\eta_{\rm th} = -\langle \mathrm{w}_{\rm tot}\rangle/\langle q_h\rangle$. To investigate the work fluctuations, we obtain the characteristic functions of the work probability distribution along the unitary compression and expansion as $G_{\rm com}(u) = \mathrm{Tr}\{U_{ch}\exp(-iuH_{t_0})\rho_{t_0}[\exp(-iuH_{t_1})U_{ch}]^\dagger\}$, and $G_{\rm exp}(u) = \mathrm{Tr}\{U_{hc}\exp(-iuH_{t_2})\rho_{t_2}[\exp(-iuH_{t_3})U_{hc}]^\dagger\}$, respectively, where $U_{ch}$ and $U_{hc}$ were defined below Eq. (9). Since no work is produced along the two isochoric strokes along each cycle, the characteristic function for the total work produced can be written as the product of characteristic functions for the two driven strokes, leading to $G(u) = G_{\rm com}(u)G_{\rm exp}(u)$ [2]. The average work and the work fluctuation can be determined according to $\langle \mathrm{w}_{\rm tot}\rangle = -i\frac{\partial \ln G(u)}{\partial u}|_{u=0}$ and $\delta \mathrm{w}^2_{\rm tot} = -\frac{\partial^2 \ln G(u)}{\partial u^2}|_{u=0}$, respectively. The relative fluctuation of power is then obtained by using $\sqrt{\delta P^2}/P = -\sqrt{\delta \mathrm{w}^2_{\rm tot}}/\langle \mathrm{w}_{\rm tot}\rangle$.

As an example, we see in Fig. 10(a) that the thermodynamic efficiency $\eta_{\rm th}$ as a function of thermalization time $\tau_h$ oscillates due to the interference between the residual coherence after the second stroke and the coherence generated in the third stroke and that the efficiency may surpass the Otto limit in the finite-time isochoric stroke where coherence is only partially erased. The thermodynamic efficiency $\eta_{\rm th}$ increases as driving time $\tau_{\rm dri}$ increases, though not monotonically, as shown in Fig. 10(b). The oscillation of the efficiency in Fig. 10(b) originates from the quantum inner friction along the two unitary strokes. We also observe from Figs. 10(c) and 10(d) that the squeezing leads to an increase in both power output and efficiency. Finally, the squeezing can enhance the machine stability as the relative power fluctuations decreases as squeezing parameter increases, as can been seen in Fig. 11. These suggest that the findings of our study in the main text based on a spin system can thus be translated into the case of the harmonic system.


[1] R. J. de Assis, T. M. de Mendonca, C. J. Villas-Boas, A. M. de Souza, R. S. Sarthour, I. S. Oliveira, and N. G. de Almeida, Efficiency of a quantum Otto heat engine operating under a reservoir at effective negative temperatures, Phys. Rev. Lett. **122**, 240602 (2019).

[2] J. P. S. Peterson, T. B. Batalhão, M. Herrera, A. M. Souza, R. S. Sarthour, I. S. Oliveira, and R. M. Serra, Experimental characterization of a spin quantum heat engine, Phys. Rev. Lett. **123**, 240601 (2019).

[3] J. Klatzow, J. N. Becker, P. M. Ledingham, C. Weinzetl, K. T. Kaczmarek, D. J. Saunders, J. Nunn, I. A. Walmsley, R. Uzdin, and E. Poem, Experimental demonstration of quantum effects in the operation of microscopic heat engines, Phys. Rev. Lett. **122**, 110601 (2019).

[4] M. Campisi and R. Fazio, The power of a critical heat engine, Nat. Commun. **7**, 11895 (2016).

[5] K. Zhang, F. Bariani, and P. Meystre, Quantum optomechanical heat engine, Phys. Rev. Lett. **112**, 150602 (2014).

[6] M. O. Scully, K. R. Chapin, K. E. Dorfman, M. B. Kim, and A. Svidzinsky, Quantum heat engine power can be increased by noise-induced coherence, Proc. Natl. Acad. Sci. USA **108**, 15097 (2011).

[7] W. Niedenzu, V. Mukherjee, A. Ghosh, A. G. Kofman, and G. Kurizki, Universal thermodynamic limit of quantum engine efficiency, Nat. Commun. **9**, 165 (2018).

[8] P. A. Camati, J. F. G. Santos, and R. M. Serra, Coherence effects in the performance of the quantum Otto heat engine, Phys. Rev. A **99**, 062103 (2019).

[9] A. Winter and D. Yang, Operational resource theory of coherence, Phys. Rev. Lett. **116**, 120404 (2016).

[10] K. Korzekwa, M. Lostaglio, J. Oppenheim, and D. Jennings, The extraction of work from quantum coherence, New J. Phys. **18**, 023045 (2016).

[11] K. Brandner, M. Bauer, and U. Seifert, Universal coherence-induced power losses of quantum heat engines in linear response, Phys. Rev. Lett. **119**, 170602 (2017).

[12] S. Rahav, U. Harbola, and S. Mukamel, Heat fluctuations and coherences in a quantum heat engine, Phys. Rev. A **86**, 043843 (2012).

[13] R. Uzdin, A. Levy, and R. Kosloff, Equivalence of quantum heat machines, and quantum-thermodynamic signatures, Phys. Rev. X **5**, 031044 (2015).

[14] K. E. Dorfman, D. Z. Xu, and J. S. Cao, Efficiency at maximum power of a laser quantum heat engine enhanced by noise-induced coherence, Phys. Rev. E **97**, 042120 (2018).

[15] G. Francica, F. C. Binder, G. Guarnieri, M. T. Mitchison, J. Goold, and F. Plastina, Quantum coherence and ergotropy, Phys. Rev. Lett. **125**, 180603 (2020).

[16] A. Streltsov, G. Adesso, and M. B. Plenio, Colloquium: Quantum coherence as a resource, Rev. Mod. Phys. **89**, 041003 (2017).

[17] T. Guff, S. Daryanoosh, B. Q. Baragiola, and Alexei Gilchrist, Power and efficiency of a thermal engine with a coherent bath, Phys. Rev. E **100**, 032129 (2019).

[18] M. O. Scully, M. S. Zubairy, G. S. Agarwal, and H. Walther, Extracting work from a single heat bath via vanishing quantum coherence, Science **299**, 862 (2003).

[19] T. Zhang, W. T. Liu, P. X. Chen, and C. Z. Li, Four-level entangled quantum heat engines, Phys. Rev. A **75**, 062102 (2007).

[20] K. Funo, Y. Watanabe, and M. Ueda, Thermodynamic work gain from entanglement, Phys. Rev. A **88**, 052319 (2013).

[21] X. L. Huang, J. L. Guo, and X. X. Yi, Nonequilibrium thermal entanglement in a three-qubit model, Phys. Rev. A **80**, 054301 (2009).

[22] Z. H. Wang, W. Wu, and Jin Wang, Steady-state entanglement and coherence of two coupled qubits in equilibrium and nonequilibrium environments, Phys. Rev. A **99**, 042320 (2019).

[23] W.-G. Wang, J. Gong, G. Casati, and B. Li, Entanglement-induced decoherence and energy eigenstates, Phys. Rev. A **77**, 012108 (2008).

[24] J. Oppenheim, M. Horodecki, P. Horodecki, and R. Horodecki, Thermodynamical approach to quantifying quantum correlations, Phys. Rev. Lett. **89**, 180402 (2002).

[25] L. del Rio, J. Åberg, R. Renner, O. Dahlsten, and V. Vedral, The thermodynamic meaning of negative entropy, Nature (London) **474**, 61 (2011).

[26] J. J. Park, K. H. Kim, T. Sagawa, and S. W. Kim, Heat engine driven by purely quantum information, Phys. Rev. Lett. **111**, 230402 (2013).

[27] Q. Chen, C. J. Zhang, S. X. Yu, X. X. Yi, and C. H. Oh, Quantum discord of two-qubit states, Phys. Rev. A **84**, 042313 (2011).

[28] J. M. Horowitz and K. Jacobs, Quantum effects improve the energy efficiency of feedback control, Phys. Rev. E **89**, 042134 (2014).

[29] K. Brandner, M. Bauer, M. T. Schmid, and U. Seifert, Coherence-enhanced efficiency of feedback-driven quantum engines, New J. Phys. **17**, 065006 (2015).

[30] P. Kammerlander and J. Anders, Coherence and measurement in quantum thermodynamics, Sci. Rep. **6**, 22174 (2016).

[31] S. Chand, S. Dasgupta, and A. Biswas, Finite-time performance of a single-ion quantum Otto engine, Phys. Rev. E **103**, 032144 (2021).

[32] Z. Y. Lin, S. H. Su, J. Y. Chen, J. C. Chen, and J. F. G. Santos, Suppressing coherence effects in quantum-measurement-based engines, Phys. Rev. A **104**, 062210 (2021).

[33] J. Roßnagel, O. Abah, F. Schmidt-Kaler, K. Singer, and E. Lutz, Nanoscale heat engine beyond the Carnot limit, Phys. Rev. Lett. **112**, 030602 (2014).

[34] J. Klaers, S. Faelt, A. Imamoglu, and E. Togan, Squeezed thermal reservoirs as a resource for a nanomechanical engine beyond the Carnot limit, Phys. Rev. X **7**, 031044 (2017).

[35] V. Singh and Ö. E. Müstecaplıoğlu, Performance bounds of nonadiabatic quantum harmonic Otto engine and refrigerator under a squeezed thermal reservoir, Phys. Rev. E **102**, 062123 (2020).

[36] Y. N. You and S. W. Li, Entropy dynamics of a dephasing model in a squeezed thermal bath, Phys. Rev. A **97**, 012114 (2018).

[37] G. Manzano, Squeezed thermal reservoir as a generalized equilibrium reservoir, Phys. Rev. E **98**, 042123 (2018).

[38] R. J. de Assis, J. S. Sales, J. A. R. da Cunha, and N. G. de Almeida, Universal two-level quantum Otto machine under a squeezed reservoir, Phys. Rev. E **102**, 052131 (2020).

[39] O. Arısoy, J. T. Hsiang, and B. L. Hu, Quantum-parametric-oscillator heat engines in squeezed thermal baths: Foundational theoretical issues, Phys. Rev. E **105**, 014108 (2022).

[40] M. Perarnau-Llobet, K. V. Hovhannisyan, M. Huber, P. Skrzypczyk, N. Brunner, and A. Acín, Extractable work from correlations, Phys. Rev. X **5**, 041011 (2015).

[41] W. Niedenzu, D. Gelbwaser-Klimovsky, A. G. Kofman, and G. kurizki, On the operation of machines powered by quantum non-thermal baths, New J. Phys. **18**, 083012 (2016).

[42] R. Dillenschneider and E. Lutz, Energetics of quantum correlations, Europhys. Lett. **88**, 50003 (2009).

[43] M. N. Bera, A. Riera, M. Lewenstein, and A. Winter, Generalized laws of thermodynamics in the presence of correlations, Nat. Commun. **8**, 2180 (2017).

[44] G. M. Andolina, M. Keck, A. Mari, M. Campisi, V. Giovannetti, and M. Polini, Extractable work, the role of correlations, and asymptotic freedom in quantum batteries, Phys. Rev. Lett. **122**, 047702 (2019).

[45] L. Buffoni, A. Solfanelli, P. Verrucchi, A. Cuccoli, and M. Campisi, Quantum measurement cooling, Phys. Rev. Lett. **122**, 070603 (2019).

[46] C. Elouard, D. Herrera-Martí, B. Huard, and A. Auffèves, Extracting work from quantum measurement in Maxwell's demon engines, Phys. Rev. Lett. **118**, 260603 (2017).

[47] C. Elouard and A. N. Jordan, Efficient quantum measurement engines, Phys. Rev. Lett. **120**, 260601 (2018).

[48] J. H. Wang, J. Z. He, and Y. L. Ma, Finite-time performance of a quantum heat engine with a squeezed thermal bath, Phys. Rev. E **100**, 052126 (2019); H. G. Liu, J. Z. He, and J. H. Wang, Optimized finite-time performance of endoreversible quantum Carnot machine working with a squeezed bath, J. Appl. Phys. **131**, 214303 (2022).

[49] B. Xiao and R. f. Li, Finite time thermodynamic analysis of quantum Otto heat engine with squeezed thermal bath, Phys. Lett. A **382**, 3051 (2018); Y. C. Zhang, Optimization performance of quantum Otto heat engines and refrigerators with squeezed thermal reservoirs, Physica A **559**, 125083 (2020); R. J. de Assis, J. S. Sales, U. C. Mendes, and N. G. de Almeida, Two-level quantum Otto heat engine operating with unit efficiency far from the quasi-static regime under a squeezed reservoir, J. Phys. B: At. Mol. Opt. Phys. **54**, 095501 (2021).

[50] G. Manzano, F. Galve, R. Zambrini, and J. M. R. Parrondo, Entropy production and thermodynamic power of the squeezed thermal reservoir, Phys. Rev. E **93**, 052120 (2016).

[51] K. Sekimoto, *Stochastic Energetics* (Spinger, Springer, 2010).

[52] U. Seifert, Stochastic thermodynamics, fluctuation theorems and molecular machines, Rep. Prog. Phys. **75**, 126001 (2012).

[53] Q. Bouton, J. Nettersheim, S. Burgardt, D. Adam, E. Lutz, and A. Widera, A quantum heat engine driven by atomic collisions, Nat. Commun. **12**, 2063 (2021).

[54] A. Smith, Y. Lu, S. M. An, X. Zhang, J. N. Zhang, Z. P. Gong, H. T. Quan, C. Jarzynski, and K. Kim, Verification of the quantum nonequilibrium work relation in the presence of decoherence, New J. Phys. **20**, 013008 (2018).

[55] H. Ge and H. Qian, Physical origins of entropy production, free energy dissipation, and their mathematical representations, Phys. Rev. E **81**, 051133 (2010).

[56] G. E. Crooks, Nonequilibrium measurements of free energy differences for microscopically reversible Markovian systems, J. Stat. Phys. **90**, 1481 (1998).

[57] A. M. Timpanaro, G. Guarnieri, J. Goold, and G. T. Landi, Thermodynamic uncertainty relations from exchange fluctuation theorems, Phys. Rev. Lett. **123**, 090604 (2019).

[58] S. Saryal and B. K. Agarwalla, Bounds on fluctuations for finite-time quantum Otto cycle, Phys. Rev. E **103**, L060103 (2021).

[59] H. Touchette, The large deviation approach to statistical mechanics, Phys. Rep. **478**, 1 (2009).

[60] G. Verley, T. Willaert, C. Van den Broeck, and M. Esposito, Universal theory of efficiency fluctuations, Phys. Rev. E **90**, 052145 (2014).

[61] S. K. Manikandan, L. Dabelow, R. Eichhorn, and S. Krishnamurthy, Efficiency fluctuations in microscopic machines, Phys. Rev. Lett. **122**, 140601 (2019).

[62] V. Holubec and A. Ryabov, Cycling tames power fluctuations near optimum efficiency, Phys. Rev. Lett. **121**, 120601 (2018).

[63] T. Denzler and E. Lutz, Efficiency fluctuations of a quantum heat engine, Phys. Rev. Res. **2**, 032062(R) (2020).

[64] G. Jiao, Y. Xiao, J. He, Y. Ma, and J. Wang, Quantum Otto refrigerators in finite-time cycle period, New J. Phys. **23**, 063075 (2021).

[65] G. Verley, M. Esposito, T. Willaert and C. Van den Broeck, The unlikely Carnot efficiency, Nat. Commun. **5**, 4721 (2014).

[66] J. H. Jiang, B. K. Agarwalla, and D. Segal, Efficiency statistics and bounds for systems with broken time-reversal symmetry, Phys. Rev. Lett. **115**, 040601 (2015).

[67] T. Denzler and E. Lutz, Efficiency large deviation function of quantum heat engines, New J. Phys. **23**, 075003 (2021).

[68] G. Q. Jiao, S. B. Zhu, J. Z. He, Y. Ma, and J. H. Wang, Fluctuations in irreversible quantum Otto engines, Phys. Rev. E **103**, 032130 (2021).

[69] R. Luo, G. Benenti, G. Casati, and J. Wang, Thermodynamic bound on heat-to-power conversion, Phys. Rev. Lett. **121**, 080602 (2018).

[70] J. Lu, Z. Wang, J. Peng, C. Wang, J.-H. Jiang, and J. Ren, Geometric thermodynamic uncertainty relation in a periodically driven thermoelectric heat engine, Phys. Rev. B **105**, 115428 (2022).

[71] B. Gardas and S. Deffner, Thermodynamic universality of quantum Carnot engines, Phys. Rev. E **92**, 042126 (2015).

[72] R. Kosloff and A. Levy, Quantum heat engines and refrigerators: Continuous devices, Annu. Rev. Phys. Chem. **65**, 365 (2014).

[73] J. Gonzalez-Ayala, J. Guo, A. Medina, J. M. M. Roco, and A. C. Hernández, Energetic self-optimization induced by stability in low-dissipation heat engines, Phys. Rev. Lett. **124**, 050603 (2020).

[74] P. Pietzonka and U. Seifert, Universal trade-off between power, efficiency, and constancy in steady-state heat engines, Phys. Rev. Lett. **120**, 190602 (2018).

[75] Y. Rezek and R. Kosloff, The quantum harmonic Otto cycle, Entropy **19**, 136 (2017).

[76] U. Weiss, *Quantum Dissipative Systems* (World Scientific, Singapore, 2012), Vol. 13.

[77] H.-P. Breuer and F. Petruccione, *The Theory of Open Quantum Systems* (Oxford University Press on Demand, New York, 2002).

[78] R. Srikanth and S. Banerjee, Squeezed generalized amplitude damping channel, Phys. Rev. A **77**, 012318 (2008).

[79] P. Solinas and S. Gasparinetti, Full distribution of work done on a quantum system for arbitrary initial states, Phys. Rev. E **92**, 042150 (2015).

[80] P. P. Hofer and A. A. Clerk, Negative full counting statistics arise from interference effects, Phys. Rev. Lett. **116**, 013603 (2016).

[81] T. Baumgratz, M. Cramer, and M. B. Plenio, Quantifying coherence, Phys. Rev. Lett. **113**, 140401 (2014).

[82] V. Vedral, The role of relative entropy in quantum information theory, Rev. Mod. Phys. **74**, 197 (2002).

[83] M. Esposito and C. Van den Broeck, Three faces of the second law. I. Master equation formulation, Phys. Rev. E **82**, 011143 (2010).

[84] L.-L. Yan, J.-W. Zhang, M.-R. Yun, J.-C. Li, G.-Y. Ding, J.-F. Wei, J.-T. Bu, B. Wang, L. Chen, S.-L. Su *et al.*, Experimental verification of dissipation-time uncertainty relation, Phys. Rev. Lett. **128**, 050603 (2022).

[85] D. von Lindenfels, O. Grab, C. T. Schmiegelow, V. Kaushal, J. Schulz, M. T. Mitchison, J. Goold, F. Schmidt-Kaler, and U. G. Poschinger, Spin heat engine coupled to a harmonic-oscillator flywheel, Phys. Rev. Lett. **123**, 080602 (2019).

[86] Y. Wu and X. Yang, Jaynes-Cummings model for a trapped ion in any position of a standing wave, Phys. Rev. Lett. **78**, 3086 (1997).

[87] F. Curzon and B. Ahlborn, Efficiency of a Carnot engine at maximum power output, Am. J. Phys. **43**, 22 (1975).

[88] Like squeezing, the quantum coherence and correlation change the diagonal and nondiagonal matrix elements and modify the detailed balance between the two energy levels, thereby effectively changing the temperature of the system [17,18,42]. This calls for an extension of the quantum nanoengines to nonequilibrium reservoirs in presence of quantum coherence and correlation.

[89] Y. Oono and M. Paniconi, Steady state thermodynamics, Prog. Theor. Phys. Suppl. **130**, 29 (1998).

[90] T. Hatano and S. I. Sasa, Steady-state thermodynamics of Langevin systems, Phys. Rev. Lett. **86**, 3463 (2001).

[91] J. M. Horowitz and T. Sagawa, Equivalent definitions of the quantum nonadiabatic entropy production, J. Stat. Phys. **156**, 55 (2014).

[92] S. Deffner and E. Lutz, Information free energy for nonequilibrium states, arXiv:1201.3888.

[93] S. Deffner and C. Jarzynski, Information processing and the second law of thermodynamics: An inclusive, Hamiltonian approach, Phys. Rev. X **3**, 041003 (2013).